ISSN 0972-0480 • Vol. 25 No. 7 • July 2022

IIM METAL NEWS

A monthly publication of The Indian Institute of Metals

IIM METAL NEWS

Vol. 25 No. 7 July 2022

Chief Editor
Dr. N Eswara Prasad

Printed and Published by
Shri Kushal Saha, Secretary General IIM,
on behalf of "The Indian Institute of Metals", and
printed at Print Max, 44, Biplabi Pulindas Street, Kolkata-700009 and
published at 'Metal House', Plot 13/4, Block AQ, Sector V, Salt Lake, Kolkata-700091, West Bengal, India

E-mail: secretarygeneral.iim@gmail.com, iimmetalnews@yahoo.com
Phone: 033-2367 9768 / 2367 5004
Website: www.iim-india.net
Fax: (033) 2367 5335
Facebook - https://www.facebook.com TheIndianInstituteofMetals/
Instagram - https://www.instagram.com/indianinstituteofmetals/
LinkedIn - https://www.linkedin.com/company/the-indian-institute-of-metals/
Twitter - https://twitter.com/iimetals_india

THE INDIAN INSTITUTE OF METALS

Interview TATA STEEL CEO & MD Mr. T V Narendran

Mr. T V Narendran
CEO & MD, TATA STEEL

How do you envision the Indian steel industry to grow in the next decade?

The prospects for the Indian steel industry look good over the medium to long term. India has traditionally had consumption-led growth. However, over the last few years, the government's focus on infrastructure is leading to more steel-intensive growth. India is also an ideal Country for steel manufacturing because of locally available Iron Ore and a large growing market for steel. So from all perspectives, the prospects of the Indian steel industry look good and I see both consumptions of steel and the production of steel growing for decades to come. India also has a great opportunity to be a strong player in the export markets as it is a more competitive place to produce steel than countries like China, Japan, and Korea which together export more than 120 million tonnes of steel today. The steel industry also creates jobs in some of the poorest parts of the country and should be encouraged to invest and grow and make steel not only for India but for the world.

What are the technological advancements that can make steel industry more sustainable?

Today, most of the steel in the world is produced using iron ore and coal. The next commonly used method is by melting steel scrap using electric energy. The steel industry currently accounts for about 8% of greenhouse gas emissions in the world. To transition to a greener future we need to substitute coal with gas and then with hydrogen. But for this, we need to have plenty of gas and hydrogen available at competitive prices. The carbon footprint of steel making by melting steel scrap is about 20% of the carbon footprint of making steel using Iron ore and coal. If the source of energy for melting scrap is green then the carbon footprint becomes almost negligible. But this process route will be limited by the amount of scrap that is available in the world. In addition to the above, we also need to invest in technologies that can capture and use or store the CO_2 that is emitted when you make steel using iron ore and coal. Globally transition to making green steel has started in Europe because the policy framework in Europe is supporting this transition. Steel companies in other regions around the world are investing in making this transition and Tata steel also has multiple projects in both Europe and in India to do the same as the Tata group Tata steel has itself a goal to become net zero by 2045.

Given that steel is infinitely recyclable it has a great future in a world that is looking for greater resource efficiency.

How has the steel industry been affected by unforeseen events like COVID-19 and Russia-Ukraine conflict?

Both these events have had a very significant impact on our industry. COVID-19 disrupted economic activity across the world and we are an industry that is very dependent on economic activity. The steel industry also has a very long supply chain with both Raw materials and critical consumables coming from different parts of the world. So the resilience of the companies and their supply chains were tested during the pandemic.

The Russia-Ukraine conflict also had a material impact on our industry. Russia and Ukraine are big exporters of steel and so the conflict disrupted the supply of steel to many parts of the world. Russia is also a big exporter of coal and so conflict led to an escalation of coal prices across the world. Many industries in Europe were dependent on the supply of critical consumables either from Russia or Ukraine and hence many of our customers also got impacted. The conflict has also distracted many countries from their focus on the economic recovery post-Covid and as a consequence growth prospects for the world economy has dimmed considerably. I do believe that both these events have also created an opportunity for India to emerge as an alternate source and an alternate market for many global companies.

What do you think about the metallurgical education in India given that IITs are preferring Materials Science over Metallurgy?

Metallurgy is a part of material science. We have to accept the fact that the world around us is changing and we also have to change with the times. The world will look for greener and cleaner materials and that means we have to rethink both applications as well as the process of production. We will also increasingly see more and more composite structures and the use of multiple materials to find the most optimal solution for our customers. Manufacturing itself is going to get disrupted with the scaling up of additive manufacturing. As an industry and as an Indian Institute of Metals we need to work with the younger demographic to attract them to material science and metallurgy.

What is exciting is also that there are a lot of start-ups working in this space and we need to leverage them better as well. Tata steel itself has a dedicated vertical now working on new materials like fiber-reinforced polymers, graphene, and ceramics. I do believe that material science and metallurgy will continue to be very important in finding the solutions for a sustainable future.

What are your thoughts to make academia and industry work together in India?

Every strong manufacturing economy has embedded in it a deep relationship between academia and industry. While in India too academia and industry work together I do believe that a lot more can be done. Institutions like The Indian Institute of Metals can play a very important role in this regard. We need to identify industrial problems where academia can contribute effectively and also look at ideas in the lab that can be scaled up by industry. The transition to a greener and cleaner future also creates multiple opportunities for Academia and the Industry to work together. The start-up ecosystem is also a great opportunity for entrepreneurs, academia, and industry to come together to find innovative solutions for the problems of today and tomorrow.

How is Tata Steel preparing for the future with respect to global steel demand and sustainability?

Tata Steel is currently in the midst of a journey to become future-ready culturally, structurally, and financially. We are transforming ourselves to become a knowledge-intensive and innovative organization committed to demonstrating excellence at all touch points. Our focus is to grow in India to double our capacity during this decade. In Europe, our focus will be to transition to making greener steel as required by customers there and supported by the policies there as well. In India also we have several initiatives in place and we continue to be a benchmark as well as far as the carbon footprint is concerned. We are also setting up recycling facilities in North, West, and South India to supplement our iron ore and coal-based steel production in the east. We are committed to becoming net zero by 2045. Our vision is to be a benchmark in value creation and corporate citizenship and we stay committed to pursuing and realizing that vision.

****

Special Feature Company Profile of TATA Steel Ltd.

Piloting the Nation's Roadmap of Self-Reliance

PAST

Our journey began in 1867, when the global consumption of steel was only 0.5 million tonnes. Jamshetji Nusserwanji Tata, our founding father, envisioned setting up a steel plant in India. Tata Steel, since its inception, has been a resolute partner to nation-building: not only on the strength of its businesses, but through its philanthropic contributions in the areas of healthcare, education, sports, technology, infrastructure and diversity & inclusion.

PRESENT

Our ambition is to be the most respected and valuable steel company in the world and driven by our deep desire to grow in India, we acquired key assets that promised long-term value and hence, from a single site at Jamshedpur, we have expanded. Apart from our very own greenfield investment in Kalinganagar, where we are currently accelerating the 5 million tonnes per annum flat products expansion programme, we have acquired Bhusan Steel (now Tata Steel Meramandali), Usha Martin and Neelachal Ispat Nigam Limited (both part of Tata Steel Long Products now) and very recently, Rohit Ferrro Tech Ltd. These strategic acquisitions will help strike a balance in our business portfolio and strengthen our foothold in the segments of Flat Products, Long Products and Ferro Alloys.

FUTURE

Looking ahead means getting into downstream businesses, services and solution-oriented ventures and exploring new materials, to beat the cyclicality of legacy business.

In the past few years, we have launched various innovative products and services and have augmented our focus on solution-oriented direct-to-use offerings for our customers, like Tata Pravesh doors, Nest-In prefabricated construction, SmartFab welded wire mesh, Tata Tiscon ReadyBuild customised rebar solutions, etc. These new businesses, as they scale up, define how steel will be used in construction in years to come. By 2030, a substantial part of Tata Steel's revenue shall come from such downstream businesses and new ventures.

We have selected to work with three composite materials that have unexplored possibilities, namely polymer matrix with fibre reinforcement, graphene and advanced ceramics. We are entering into several collaborations, in order to develop know-how and potential of these. By 2030, we aspire to capture at least 10-12 percent of these markets.

We have also taken steps to further strengthen customer relationships by leveraging digital tools. Our e-commerce platform, *Aashiyana*, is growing manifold and the annual turnover in FY'22 stands at ₹1,468 crore.

Our growth aspirations are aggressive and the ambition is to go to 40 million tonnes by 2030 and between now and 2025, we would have made the plans for the third phase of expansion at Kalinganagar as well as in Meramandali.

The industrial workforce of the future needs to be skilled in digital technologies, in order to stay relevant. Our digital journey also embedded in us the need, passion and momentum to innovate. Three of our plants - Jamshedpur, Kalinganagar and Ijmuiden are now in the global lighthouse network - a recognition from the prestigious World Economic Forum, as well as Industrial Benchmarks from Gartner amongst others.

As an organisation, we recognise sustainability as a crucial part of our existence. With our Prime Minister having announced 2070 as the target year for India to achieve net zero carbon emissions, it is imperative for us to take decisive steps towards a lower carbon footprint.

Substantial work is being done by us in managing natural capital through our strategies on low carbon transition, reducing dependence on freshwater consumption, pollution control, maximising value from waste, exploring opportunities in the circular economy and enhancing biodiversity across the value chain. We will continue to explore multiple options to gear ourselves towards a greener future.

We are striving towards minimising air emissions to ensure healthy air quality in the communities we operate. Our continuous efforts have resulted in overall reduction of 29% in stack dust emission intensity since FY18. Also, the specific freshwater consumption of our Jamshedpur Works (@2.18 m3/tcs in FY22) is one of the lowest in steel industry in India.

We have initiated the trial for continuous injection of coal bed methane (CBM) gas, in one of the Blast Furnaces at our Jamshedpur Works, making it the first such instance in the world. We are also the first company to have commissioned a 0.5 MTPA steel recycling plant (Scrap collection and Shredding facility) at Rohtak (Delhi-NCR) and our future plans aim to replicate such facilities in the west and south of India as well.

Circular economy models to reduce the amount of raw materials consumed, reuse, refurbish and recycle, are being adopted, along with systematic and consistent deployment of safety practices, in order to help us achieve 'zero harm'. In FY 2021-22, our Jamshedpur and Kalinganagar plants achieved 100% Solid Waste Utilisation, while horizontal deployment of best practices in Meramandali helped achieve 97% solid waste utilisation.

Safety being yet another core value, we have embarked on a journey of cultural change. We have leveraged artificial intelligence (AI) to institute intelligent mechanisms in our areas of operations to ensure maximum safety.

Changing demography and evolving expectations of the new generation nudge us to reimagine the future of work, workspace, and human resource. We were pioneers in this field a century ago, with many 'first-evers' - and again, with a move by the way of recruitment of transgenders, the Company has evolved as a global torchbearer.

Tata Steel is credited with several prestigious awards and important recognitions, over the last many years. We were certified by Great Place to Work® for the fifth year in a row and recognised as one of the World's Most Ethical Companies for 2021, by the Ethisphere Institute. Furthermore, worldsteel has recognised us as 2022 Steel Sustainability Champions, for the fifth consecutive year and have been acknowledged amongst the Top 10 Sustainable organisations of India, by Hurun Research Institute, in the 2021 Capri Global Capital Hurun India Impact 50. We have also joined the Taskforce on Nature-related Financial Disclosures (TNFD) as its Member, in order to support a shift in global financial flows away from nature-negative outcomes toward nature-positive outcomes.

As we keep growing both organically and inorganically, besides building capacity, we will be focusing on developing, unlocking and monetising knowledge, in order to remain the 'organisation of choice', across segments. We are looking at community engagement beyond the prism of CSR, by understanding how we can cater to their requirements through our innovative products and services as well as meaningful solutions, so as to bring about a better today and a developing tomorrow.

We have been a part of the nation building journey for over a hundred years and we continue to commit ourselves to contribute significantly to the *"Atma Nirbhar Bharat"* ambition of the nation, in the years to come.

Tata Steel Jamshedpur plant, Jharkhand

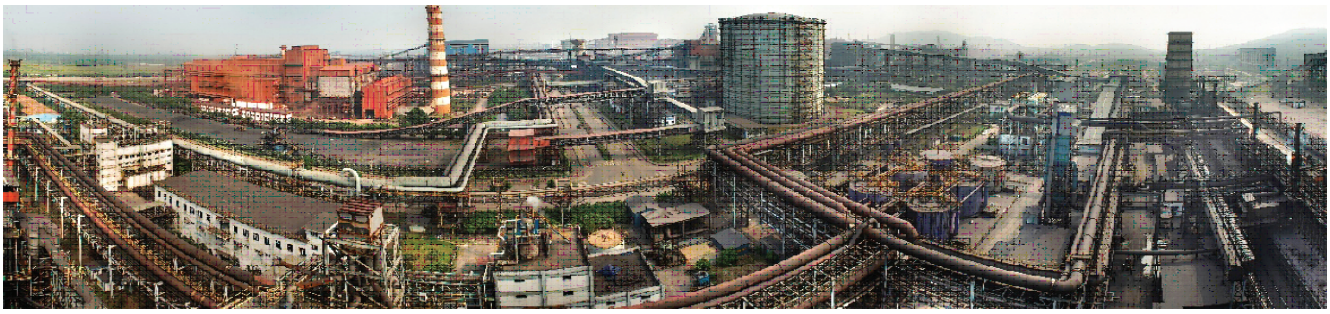

Tata Steel Kalinganagar plant, Odisha

Tata Steel's solution-oriented direct-to-use offerings 'Tata Pravesh': Double rebate embossed door with swing & slide window

Tata Steel's solution-oriented direct-to-use offerings: Nest-In prefabricated construction

Product portfolio: Tata Steel

Certified by Great Place to Work® for the fifth year in a row

Tata Steel has been recognised as one of the Top 25 most innovative Indian Companies for its product, process, and business innovation practices across steel value chain

Tata Steel have been acknowledged amongst the Top 10 Sustainable organisations of India, by Hurun Research Institute

****

Technical Article

Analysis of Interphase Precipitates in an Advanced High Strength Steel through TEM-TKD Hybrid Technique

Bhagyaraj Jayabalan, Akula Durga Prasad and Subrata Mukherjee*

Abstract

Nano scale interphase precipitates strengthened advanced high strength steels (AHSSs) have revolutionized the development of ultrahigh tensile steels. The shape, size, volume fraction and distribution of such fine precipitates (average size of <10 nm) significantly influence the mechanical properties of these grades. Therefore, advanced techniques like SEM and TEM have been extensively used to characterize microstructure and precipitates of such a grade in the present study. However, traditionally aforesaid advanced techniques analyse different areas/populations of same steel grades and therefore one to one correlation is not possible from studies done by subsequent techniques. Future trend in advanced characterization is Correlative Microscopy i.e., same area/grain is observed by different techniques to extract additional information. Correlative study using TEM and TKD (Transmission-Kikuchi Diffraction) in combination on an interphase precipitate strengthen AHSS have been performed to understand its microstructure and precipitation behaviour. The characteristics of precipitates and its distribution was studied using traditional TEM, whereas the crystallographic information such as grain boundary character, micro-texture, misorientation distribution was obtained through TKD analysis. The pre-existing dislocation in the microstructure significantly influenced the nucleation and growth of the precipitates. Correlative microscopic analysis enabled to understand the precipitation characteristics in a better manner, which may be used for grain boundary engineering to optimize the desired microstructure.

Keywords: AHSS, Interphase precipitates, TEM, TKD

1.0 Introduction

Nano precipitates strengthened AHSSs emerged as an attractive material for automobile industries as it offers excellent combination of mechanical properties and ability to design complex structural components. The desired combination of strength and ductility is generally tailored through microstructure and precipitation process. In AHSS, ferrite phase is strengthened by introducing fine scale precipitates through adding micro alloys such as Titanium, Vanadium, Niobium and Molybdenum [1-10]. The decomposition of austenite during phase transformation often observed precipitation of fine carbides [1,11,12] and this kind of precipitation referred as interphase precipitate as it occurs at the moving interface of austenite and ferrite. During the transformation of austenite into ferrite, fine scale of carbides develops at the interface by consuming the solute atoms near the interphase. The concentration gradient of the carbon aids to move the interface forward. This process occurs in repetitive steps resulting in the formation of sheets of parallel carbide precipitates [3,13]. There are several models and mechanisms such as Gray model [13], Ledge mechanism [2], bowing mechanism [6], Eutectoid mechanism, solute drag nucleation model [11], solute depletion model proposed on the nucleation and development of interphase precipitation. Each of the model provides particular characteristics of the precipitates such as morphology, direction of the growth, spacing of the bands, curvature of the lines etc., however there is no model which provides comprehensive explanation of interphase precipitation development. Recently, it has been shown that presence of numerous clusters that influence the overall precipitation process and

Tata Steel Limited, Research and Development, Jamshedpur, Jharkhand, India
Corresponding author's E-mail : *subrata.mukherjee@tatasteel.com

thereby mechanical properties of the material [14]. These carbides are generally observed at nanoscale in the range of 3-10 nm with inter-sheet spacing of 10-20nm [5]. These interphase precipitation have been realized in several microalloying steels in the form of metal carbides or carbonitrides such as V(C,N), NbC [9], (V,Cr)C [2], (NbMo)C [15], (Ti, Mo) C [3], Mo2C [1] etc. These precipitates are reported to have Baker-Nutting crystallographic orientation relationship with ferrite matrix [2].

Thermo-mechanical controlled processing (TMCP) is the most popular and cost-effective ways to produce AHSS. Traditionally hot strip mill can be used to produce it. The steel is hot-rolled above austenite-ferrite transformation temperature and then fast cooled on the run-out table prior to being coiled. The processing conditions like cooling rate and coiling temperature influence the evolution of the microstructure significantly. Higher coiling temperatures, slower cooling rate and longer holding times normally coarsen precipitates and thereby decrease the final mechanical properties of the steel. This knowledge is extremely important from precipitate growth and thereby alloy design point of view. The strength of the material is significantly influenced by the nature of the precipitates such as size, morphology, volume fraction and distribution etc. There are several attempts made by various researchers to understand the mechanisms of precipitate formation to enhance the mechanical properties of AHSS. However, the comprehensive understanding on the precipitation formation is a scare, because of the challenges associated with the characterization of nanosized precipitates and to understand the underlying mechanism.

To date, conventional TEM is the only analytical instrument to have been used extensively for these precipitation studies. However, it possesses certain limitations for quantitative analysis of the shape, size, distribution and chemical composition of nanoclusters and the fine-scale precipitate particles that form during different thermomechanical treatments of steels. These limitations arise because: (i) high dislocation density (ii) difficult to examine precipitates smaller than 5 nm size; (iii) the ferromagnetic nature of the steel sample. Additionally, the understanding of the microstructure gets limited while employing a single technique for characterization of materials due to the instrument capabilities. More importantly, region analysed in different instruments are different, therefore we get analysis of different region while testing under subsequent microscopes. It now becomes very essential to study the various microstructural features of same region using different techniques for developing comprehensive understanding about the material. Over the past decades, the analysis of the microstructure achieved a remarkable breakthrough with an advancement of characterization techniques. With advance technologies, it is now possible to broaden our understanding about the material characteristics by stretching the analysis to next level. There are several potential instruments to characterize the specific aspect of the material. Transmission electron microscope (TEM) and Transmission Kikuchi diffraction (TKD) are potential characterization technique, which in combination offers the unique characteristics of the material. TEM is widely used to study the microstructural features at nanoscale because of its very high resolution (< 1Å). Transmission Kikuchi diffraction is another variant of electron backscatter diffraction (EBSD). The main difference between TKD and EBSD is the mode of signal collection. Since the signal is collected in transmission mode, the TKD analysis requires very thin sample with electron transparent region. As compared to EBSD technique, the resolution of the TKD is much better because of the less interaction volume in the sample.

This is an attempt to carry out in-depth analysis of the precipitates using combined characterization technique by employing TEM and TKD techniques. An effort is made to analyse the same sample/area/grain under both techniques and to establish a correlative microstructural study. The results obtained using hybrid characterization technique are discussed with adequate evidence and literature support.

2.0 Experimental

The low carbon steel with nominal composition of Fe-0.08C-1.52Mn-0.41Si-0.63(V+Mo+Nb(wt.%) was selected for the present work. The as received sample was initially hot rolled between 1200^{0}C and 1000^{0}C to the thickness of 14mm. The cylindrical sample of

10 × 15 mm was prepared for thermo-mechanical experiments. The hydrawedge mobile conversion unit (MCU) equipped Gleeble 3800 simulator was used for TMP experiments. The thermomechanical simulation, schedules is mentioned elsewhere [14], consists of total strain of 1 followed by coiling at 650^{0}C for 3600s.

The samples for optical microscopy were prepared through standard metallographic sample preparation. The mirror like polished surface was etched using 5% Nital (5% Nitric acid + 95% Ethanol) and the microstructure was analysed under Leica DM6 M optical microscope.

For TEM analysis and TKD analysis, thin slices of about 800 µm were initially sectioned with a low speed Isomet cutting machine. Slices were thinned to about 100 microns using emery sheets and the discs of 3mm diameter punched out using Gatan made disc punch tool. The final preparation of the sample was done through electropolishing using Struers: Tenupol-5 twin jet electropolisher. The solution of perchloric acid mixed with ethanol in the ratio of 10:90 by volume was used as electrolyte and polishing was done at 24V by maintaining electrolytic temperature at -30^{0}C during polishing. The TEM analysis was carried out under FEI Talos F200X transmission electron microscope and the TKD analysis was performed on FEI Scios dual beam FEG (Field emission gun) scanning electron microscope. The schematic representation of EBSD, TKD and TEM is shown in **Figure 1** for better understanding.

3.0 Results and Discussion

3.1 Basic microstructure analysis

The typical microstructure of the selected AHSS observed under optical microscope and SEM is provided in **Figure 2**. The microstructure shows recrystallized grains of ferrite as dominant phase with trace amount of second phase. The ferrite grains were observed nearly equiaxed with an average size of 4.85±0.5µm. In such AHSS, the strength of the materials is primarily achieved through precipitation strengthening, therefore the microstructure expected to have fine scale precipitates in the ferrite matrix. Further microstructural and precipitation analysis was carried out using transmission electron microscope.

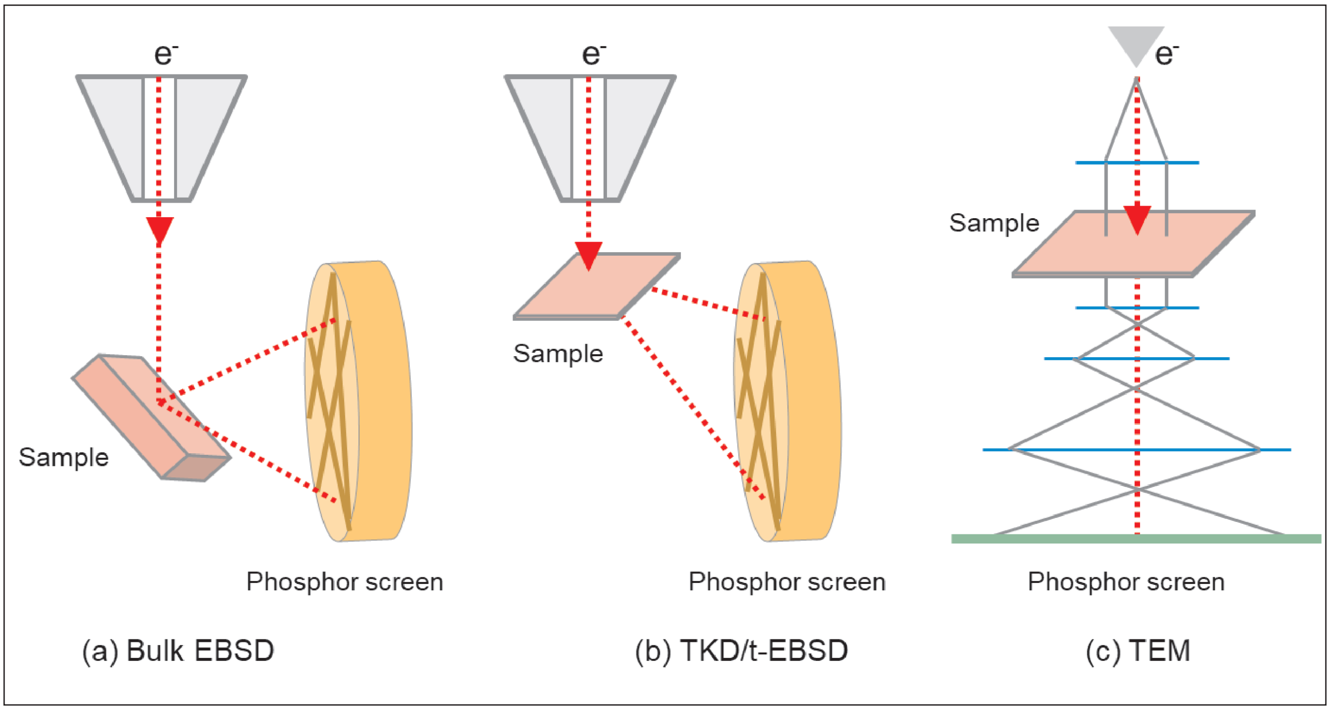

Fig. 1 : Schematic comparison of bulk EBSD, TKD and TEM techniques.

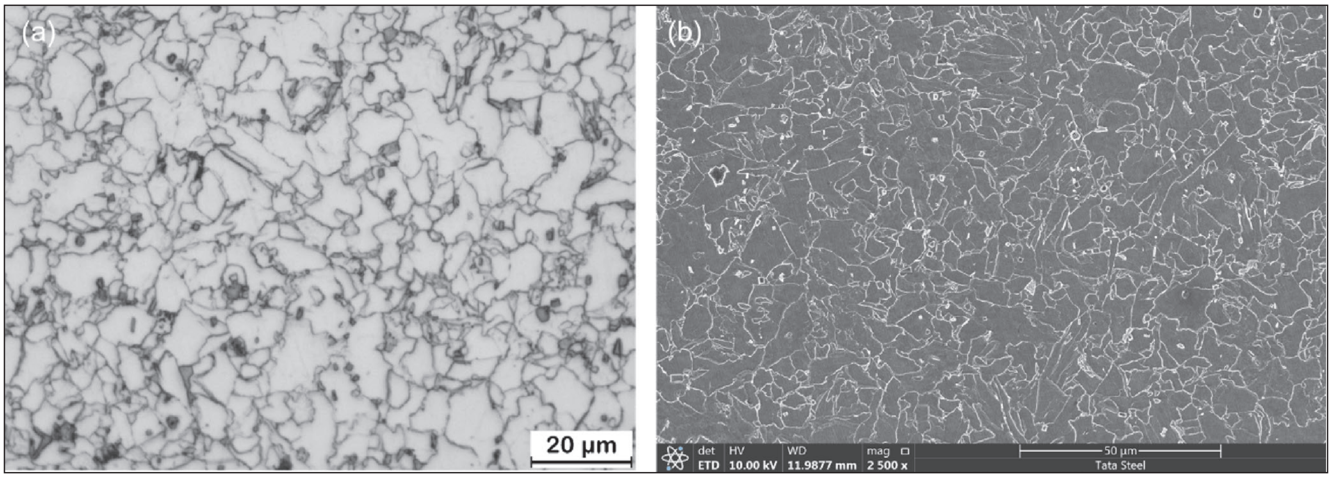

Fig. 2 : Typical microstructure of AHSS steel: (a) optical micrograph and (b) SEM micrograph.

3.2 Advance microstructural analysis using TEM

TEM is a powerful characterization tool that can be used for obtaining microstructural information at nano/atomic scale. The typical microstructural analyses which is possible only through TEM are provided in **Figure 3**. The bright field TEM micrograph in **Figure 3a** illustrating the distribution of nanoscale precipitates in the ferrite matrix. The distribution of the precipitates can be clearly seen as bright spots on the corresponding dark field micrograph shown in **Figure 3b**. It has been reported that these precipitates have orientation relationship with the ferrite matrix. To understand the crystallographic characteristics of the precipitates, selected area diffraction analysis (SADP) was performed on the region shown in **Figure 3a**. The diffraction pattern in **Figure 3c** shows the reflections of both matrix and precipitates. The strong reflections corresponding to the matrix were indexed to ferrite phase and the weak reflections are indexed to precipitates. The diffraction analysis confirms the existence of Baker-Nutting orientation relationship of $[001]\alpha//[001]vc$ between matrix and precipitates.

The precipitate was further analysed at higher magnification to reveal the periodic arrangements of the atoms. The high-resolution image in **Figure 3e** showing the lattice image of the VC precipitate wherein the column of atoms can be clearly observed. The lattice planes corresponding to (111) and (200) are marked on the micrograph shown in **Figure 3f**. The lattice planes measured from HETEM micrograph confirms the presence of VC precipitates.

3.3 Correlative microscopy analysis using TEM-TKD

Transmission Kikuchi diffraction (TKD) also referred as transmission EBSD is another potential characterization technique, which offers all the functionalities to that of EBSD analysis but with relatively higher resolution due to less sample interaction volume. Since both TEM and TKD techniques requires thin electron transparent regions, the same sample was used for both analyses. This made it possible to analyse the same sample/area/grain under both techniques and enabled to derive better microstructural correlation. Typical TKD analysis of the AHSS sample in **Figure 4** showing the IPF map and band contrast image of the microstructure. From the TKD analysis, the low angle and high angle boundaries were marked on the band contrast image **(Figure 4b)** with red and blue solid lines, respectively.

SEM based TKD analysis is limited with the resolution and further analysis of TEM is required to observe the nanoscale microstructural features. The grain subjected for TEM analysis is indicated by arrow in **Figure 5a** and same is extracted as shown in **Figure 5b**. The bright field TEM micrograph of the indicated grains is observed at low magnification and provided in **Figure 5c**. For better appreciation, the same grain observed under TKD is marked by yellow dotted line on the TEM micrograph shown in **Figure 5d**. The high magnification TEM micrograph in **Figure 5e** illustrates microstructural features in a better manner. The microstructure reveals nanoscale interphase precipitates throughout the grain. The dislocation lines, grain boundaries and precipitates distribution can be better appreciated in TEM micrograph. The periodic rows of interphase precipitates can be evidenced well in the microstructure. The interphase precipitate occurs at the moving interphase of α/γ during the phase transformation from austenite to ferrite. The rows of precipitates occur at a preferred direction of the interface movement. The interphase precipitates can be seen as rows of precipitates only at certain orientation, due to this some of the precipitates appear random at certain region. This observation

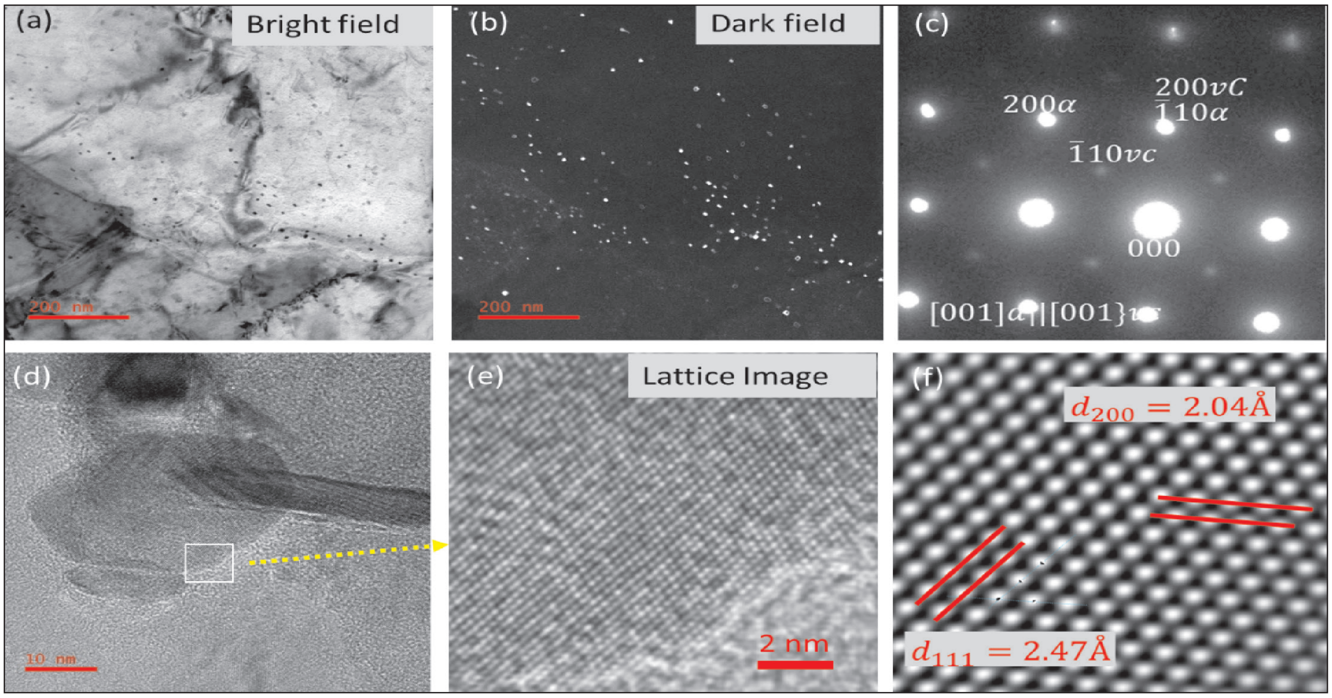

Fig. 3 : TEM analysis of AHSS showing the precipitate distribution in (a) bright filed and (b) dark field and the corresponding (c) diffraction pattern. The high resolution TEM micrograph of the precipitate (c) enlarged in (e-f) to reveal the arrangement of atoms.

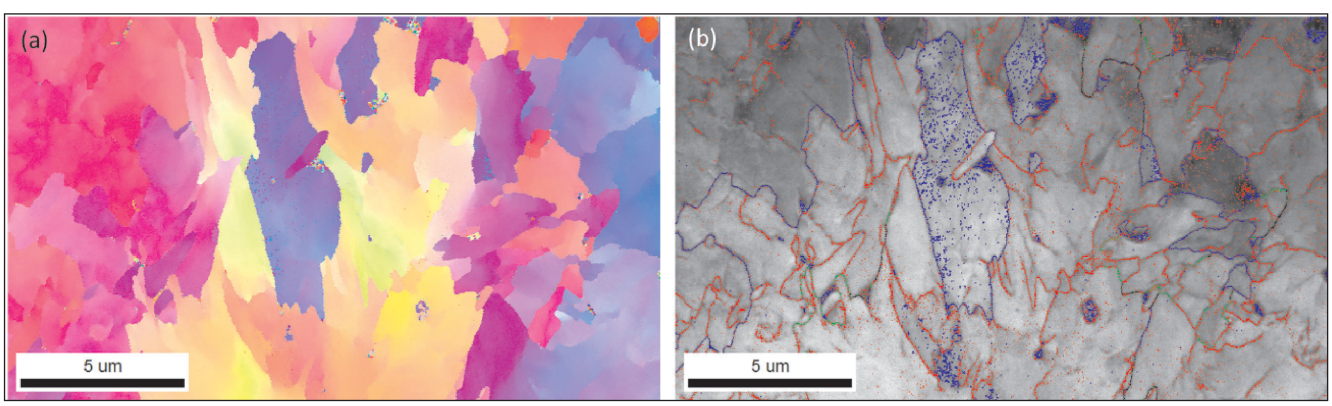

Fig. 4 : TKD analysis of the AHSS steel showing the grain morphology in the (a) IPF map and (b) band contrast map. The low angle grain boundaries and high angle grain boundaries are marked as red and blue lines, respectively.

suggests that there is in-grain misorientation within a grain. The in-grain misorientation was estimated through TKD analysis using Kernel average misorientation (KAM) tool and shown in **Figure 5c.** The colour map indicates the distribution of misorientation (in degrees) with the neighbouring pixels.

The characteristics of the various nanoscale precipitates developed in the selected AHSS is illustrated in **Figure 6**. The precipitates were observed with two types morphologies, namely spherical and fibrous precipitates. The formation of precipitates on the pre-existing defects such as grain boundary and dislocations are slightly different from the characteristics of the interphase precipitates. The morphology of the dislocation precipitates and grain boundary precipitates are indicated in **Figure 6**. It can be noted that both GB and dislocation precipitates appear to be coarser as compared to the regular interphase precipitates. The variation in the development of the precipitates can be correlated with the stored strain energy in the microstructure. The grain boundaries and dislocation line possess higher stored energy, which promotes the nucleation of precipitates much earlier than the interphase phase begins during phase transformation. This rapid coarsening of precipitates occurs via pipe diffusion. By correlating the TKD and TEM analysis, one can relate the grain boundary character with the precipitation kinetics and in this case, the grain boundary was identified as high angle grain boundary. Further detailed analysis can be carried out by correlating crystallographic characteristics such as grain boundary character, micro-texture with the development of nanoscale feature for better understanding of the precipitation kinetics.

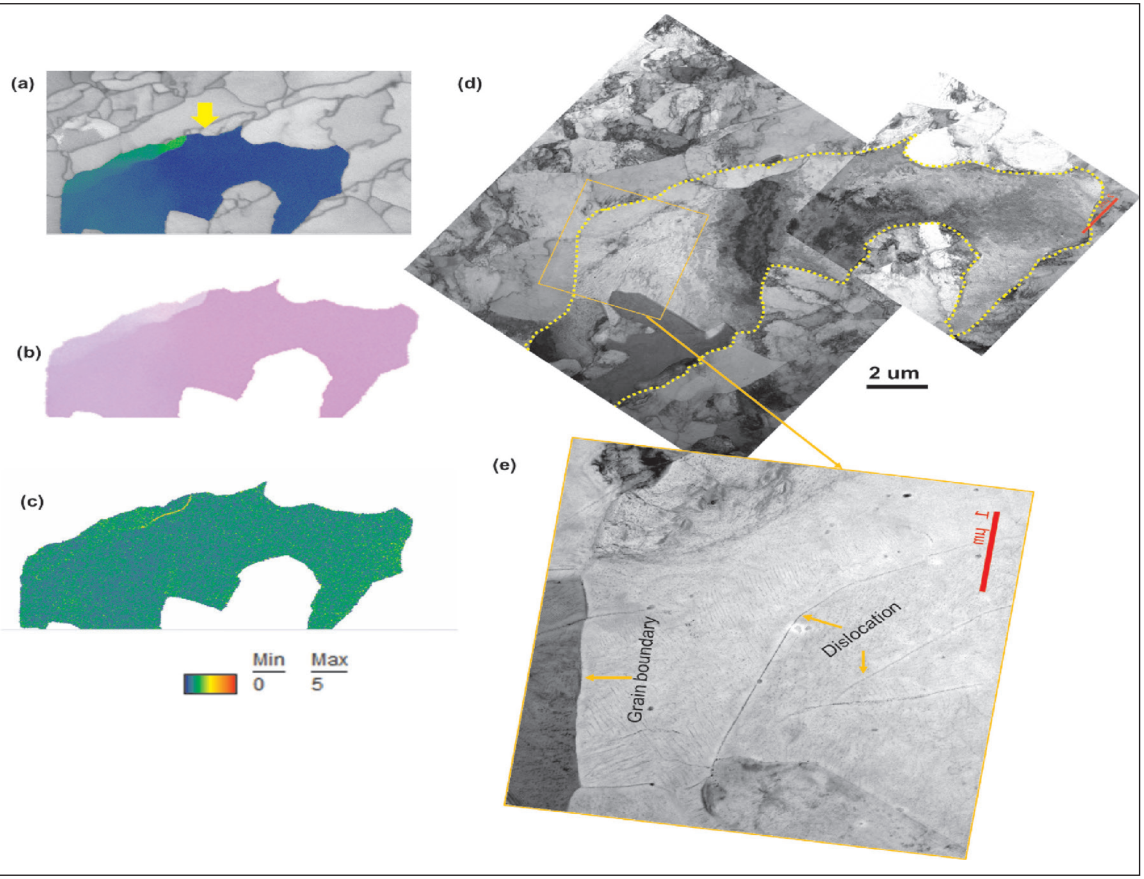

Fig. 5 : TEM-TKD analysis of a selected grain highlighted on the band contrast image in (a) and the same grain is delineated in TEM micrograph in (c). The characteristics of the interphase precipitates can be better seen in higher magnification TEM micrograph in (d).

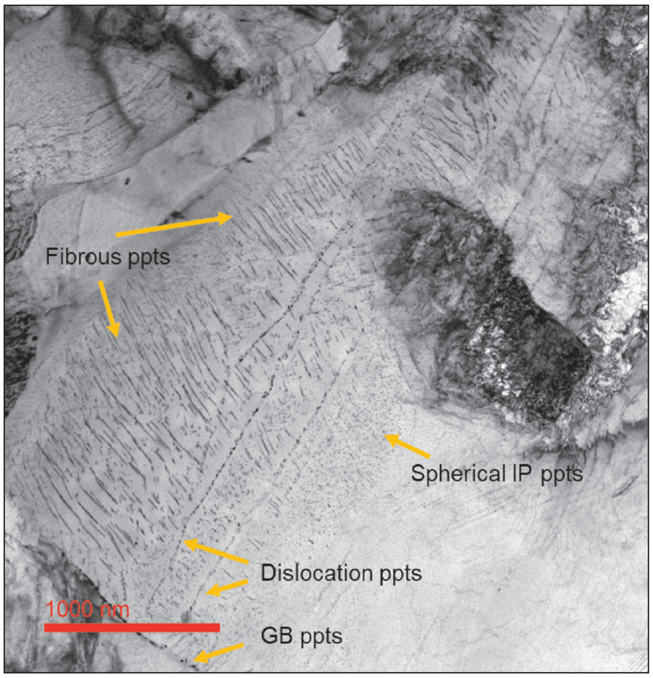

Fig. 6 : Bright field TEM micrograph illustrating various precipitates in the AHSS.

4.0 Conclusions

The following conclusions are drawn from the microstructural analysis of AHSS using TEM-TKD correlative characterization techniques.

- The pre-existing defect structures such as dislocations and grain boundaries in the microstructure significantly influence the nucleation and growth of the precipitates.
- The high angle grain boundaries and dislocations known to have higher lattice disorder, act as preferential nucleation sites for precipitates and promote the nucleation earlier than interphase precipitation and coarsens the precipitates through pipe diffusion.
- Correlative microscopy analysis using TKD and TEM enables to correlate the crystallographic characteristics of the microstructure with nanoscale features for better understanding of precipitation kinetics.

Reference

1. Davenport A, Honeycombe RWK. Precipitation of carbides at $\gamma - \alpha$ boundaries in alloy steels. Proceedings of the Royal Society of London A Mathematical and Physical Sciences. 1971; 322(1549):191-205.
2. Honeycombe R, Mehl R. Transformation from austenite in alloy steels. Metallurgical Transactions A. 1976;7(7):915-936.
3. Mukherjee S. Nanoscale precipitation in advanced high strength steels: Deakin University; 2012.
4. Mukherjee S, Timokhina I, Zhu C, et al. Three-dimensional atom probe microscopy study of interphase precipitation and nanoclusters in thermomechanically treated titanium–molybdenum steels. Acta materialia. 2013;61(7):2521-2530.
5. Mukherjee S, Timokhina I, Zhu C, et al. Clustering and precipitation processes in a ferritic titanium-molybdenum microalloyed steel. Journal of Alloys and Compounds. 2017;690:621-632.
6. Ricks R, Howell P. The formation of discrete precipitate dispersions on mobile interphase boundaries in iron-base alloys. Acta Metallurgica. 1983;31(6):853-861.
7. Batte A. Precipitation of vanadium carbide in ferrite. 1973.
8. Funakawa Y, Shiozaki T, Tomita K, et al. Development of high strength hot-rolled sheet steel consisting of ferrite and nanometer-sized carbides. ISIJ international. 2004;44(11):1945-1951.
9. Sakuma T, Honeycombe R. Microstructures of isothermally transformed Fe-Nb-C alloys. Metal science. 1984;18(9):449-454.
10. Timokhina I, Xiong X-Y, Beladi H, et al. Three-dimensional atomic scale analysis of microstructures formed in high strength steels. Materials Science and Technology. 2011;27(4):739-741.
11. Edmonds D. Occurrence of fibrous VC during transformation of an Fe-V-C steel. J Iron Steel Inst. 1972;210(5):363-365.
12. Law N, Parsons S, Howell P, et al. Crystallography of carbide precipitation at transformation interfaces during austenite decomposition in a low-alloy steel. Materials science and technology. 1987;3(8):642-648.
13. Gray J, Yeo R. Columbium carbonitride precipitation in low alloy steels with particular emphasis on precipitate row formation. ASM Trans Quart, June 1968, 61, 255-269. 1968.
14. Pradhan R, Karmakar A, Ghosh M, et al. Effect of thermomechanical processing on microstructural evolution in precipitation strengthened ferrite steel. SN Applied Sciences. 2019;1(7):1-15.
15. Okamoto R, Borgenstam A, Ågren J. Interphase precipitation in niobium-microalloyed steels. Acta Materialia. 2010;58(14):4783-4790.

****

Technical Article

Corrosion Behavior of Commercially available Galvanized Steels

Harikrishna Kancharla[1], G.K. Mandal[2], S.S. Singh[1], and K. Mondal[1]*

Abstract

Galvanized (GI) sheets provide corrosion protection to the steel substrate due to the sacrificial effect of zinc (Zn) coating, where Zn coating is consumed, and steel acts as a cathode in the electrochemical system. The present study systematically investigates and compares the microstructure, thickness, and corrosion behavior of commercially available galvanized low carbon steel sheets in the Indian market. The effect of insufficient aluminum at the substrate coating interface on the microstructure and thickness of the GI coating was studied. The electrochemical polarization behavior of the GI sheets as well as the underlying steel substrates (after removal of the galvanized layer) was tested by Tafel polarization in a freely-aerated (natural exposure of solution to the ambient atmosphere) 3.5 wt. % NaCl solution. Morphology and phase analysis of the corroded samples was performed using scanning electron microscope and X-ray diffraction, respectively. The effective sacrificial behavior of the galvanized layer for the different coated specimens was compared as a function of the layer-defects and rust composition.

Keywords : Galvanized sheets; Sacrificial anode; Microstructure; Corrosion.

1. Introduction

Steel sheets are widely used for various applications, including automobile and construction sectors, mainly due to their superior mechanical properties and affordable cost. However, steel sheets are susceptible to corrosion and require protection [1]. Metallic coatings are one of the ways to protect the steel sheet from corrosive environments and hot-dip galvanizing is one of the commercially viable Zn-coating methods for mass production [1], where a Zn-based coating is applied to the steel substrate by passing the sheet (in coil form) through a molten Zn-alloy bath. Galvanized (GI) coatings protect steel from environmental corrosion in two ways: barrier protection and galvanic protection [1, 2]. The outer layer of the GI coating predominately consists of the Zn-rich eta (η) phase, which is a solid solution of iron (Fe) in Zn with 0.03 wt. % Fe at 460 ^{0}C [1]. Most of the galvanizing baths contain a very small amount of dissolved Al (~ 0.2 wt. %) resulting in the formation of an extremely thin continuous Al-rich inhibition layer (Fe_2Al_5) at the substrate-coating interface [1]. This thin and hence more ductile inhibition layer adheres to both the steel substrate and the coating without impairing strip- formability and inhibits the formation of any detrimental hard and brittle Fe-Zn intermetallic compounds (ξ($FeZn_{13}$), δ ($FeZn_{10}$) and Γ (Fe_3Zn_{10}) in the coating [1].

The chemical composition of the steel substrate, specifically carbon (C), silicon (Si), phosphorous (P), and manganese (Mn), affects the coating microstructure, which in turn determines the corrosion response of the GI sheets [1, 3]. Moreover, the thickness and coating structure of the GI coating is primarily influenced by the Zn- bath temperature and immersion time. It has been documented that the increased bath temperature leads to increased dissolution of the steel substrate into the galvanizing bath, resulting in the formation of Fe-Zn intermetallic compounds in the coating, and contributing to increased coating thickness due to the larger specific volume [1]. Mandal et al. [4] have reported that increasing the immersion time of the

[1] Department of Materials Science and Engineering,
Indian Institute of Technology Kanpur, Kanpur-208016, India
[2] CSIR-National Metallurgical Laboratories, Jamshedpur, Jharkhand-831007, India
*Corresponding Author : Email– *kallol@iitk.ac.in*
Phone: +915122596156; Fax: +915122597505

substrate in the galvanizing bath led to increased diffusion of Fe into the Zn layer and increased the coating thickness. There have been many studies on the production of GI coatings; but a comprehensive analysis of the impact of insufficient Al at the substrate-coating interface on the microstructure and thickness of the GI coating is lacking.

The corrosion behavior of the GI sheets has been studied by many researchers [1, 2]; corrosion resistance is determined by the coating thickness, microstructure, and surface flaws. Townsend [5] has observed that the corrosion resistance of GI sheets improves as the thickness of the coating increases. The corrosion resistance of the GI coatings is determined not only by the coating thickness but also by the presence of Fe-Zn intermetallic compounds. The coating composition and microstructure also influence the corrosion resistance of GI sheets. Fe-Zn alloy coatings provide better corrosion resistance than pure Zn coatings because the former corrodes at a reduced rate in corrosive environments [6]. Fe-Zn/Fe-Al intermetallic compounds in the coating not only influence its corrosion resistance, but the Fe-Zn/Fe-Al layer at the substrate/coating interface also improves the adhesion properties of coatings. This is crucial for forming applications [1]. Dong et al. [7] have reported that the imperfections in the coating, such as pores or scratches reduced the effectiveness of cathodic protection. The corrosion resistance of GI sheets is affected by the solubility and adhesion of corrosion products produced during the exposure [8]. In the open literature, however, there is little in-depth study on the effective sacrificial behavior of GI sheets based on coating defects and rust composition. Therefore, a comprehensive study on these along with the corrosion mechanism of GI coatings in freely aerated 3.5 wt. % NaCl solution can be considered worthy of investigation.

In the present study, the microstructure, thickness, and corrosion behavior of a commercially available galvanized low carbon steel sheets have been studied. Also, the thickness of the GI coating as well as its microstructure have been examined in relation to insufficient Al at the substrate-coating interface. Furthermore, the layer defects and rust composition have been considered in determining the effective sacrificial behavior of the galvanized layer.

2. Experimental Procedure

Three samples of commercially available hot-dip galvanized steel sheets with a thickness of 1.2 mm were obtained from the Indian market (Gal A, B, and C) and served as the starting materials for the present investigation. However, the exact methods followed in the manufacture of the GI sheets were unknown, since these were purchased from the open market. The primary purpose, however, was to examine the effect of coating surface defects and rust composition on the effective sacrificial behavior of commercially available GI sheets. The chemical composition of the steel substrates of the three GI sheets was analyzed using Spectro Maxx Optical Emission Spectroscopy (OES) and is shown in Table 1.

Table 1: Chemical composition of the steel substrates (in wt. %) obtained from the Spectro Maxx OES

Elements	Steel substrate of Gal A	Steel substrate of Gal B	Steel substrate of Gal C
C	0.045	0.070	0.045
Si	0.026	0.080	0.029
Mn	0.218	0.350	0.208
P	0.017	0.019	0.011
S	0.020	0.005	0.010
Mo	0.008	0.008	0.008
Fe	99.25	99.24	99.49

For microstructural characterization of the cross-section, the GI sheets were first sectioned into small pieces (2×2 cm^2). These pieces were then mounted and ground with 2500 grit silicon carbide paper. Final polishing was performed with diamond paste (1 micron) by maintaining the standard practice for specimen-edge retention. After thorough ultrasonic cleaning, the specimens were etched with 2-3 vol. % freshly prepared Nital solution to observe the microstructure. The top surface of the steel substrate was revealed for microstructure observation by grinding the coating layer with silicon carbide papers down to 600 grit size followed by a final polishing. The microstructures of the coating layer, cross-section, and top surface of steel substrates were characterized by scanning electron microscope (SEM

Nova Nano 450) in secondary electron (SE) mode. The phases were identified using a combination of energy dispersive spectroscopy (EDX) in SEM and X-ray diffraction (XRD PANalytical). Cu-K_α radiation was used to generate XRD patterns at diffraction angles from (2θ) 20^0 to 80^0, with a grazing angle of 1^0 and a scan rate of 0.01^0/s. The coating thicknesses were determined using SEM micrographs of cross-sections. The pearlite fraction in the steel substrate of Gal B was also calculated using ImageJ software.

The electrochemical experiments were carried out on the GI coatings as well as steel substrates using PARSTAT 2263 potentiostat. A conventional round-bottom cell was used to carry out all the electrochemical experiments in a freely aerated 3.5 wt. % NaCl solution at room temperature. Prior to the electrochemical testing of samples, all the samples were cleaned with methanol. Platinum and saturated calomel electrodes (E_{SCE} = + 0.24 V) were used as counter electrode and reference electrode, respectively. The open-circuit potential (OCP) was determined after 1 h of stabilization. Following that, at a scan rate of 0.16 mV/s, Tafel polarization tests were conducted in the cathodic and anodic ranges of OCP -250 mV and OCP +250 mV, respectively. The corrosion rate was calculated using Faraday's law and using the following equation [ASTM G102] [9]:

$$\text{Corrosion rate (mm/year)} = 3.27\times\left(10^{-3}\right)\times\frac{i_{corr}}{\rho}\times EW \quad (1)$$

where, 'EW' and 'ρ' are the equivalent weight (g) and the density of the element (g/cm^3), respectively, 'i_{corr}' is the corrosion current density (μA/cm^2), which was estimated using Tafel extrapolation method. The morphology and phase analyses of the corrosion products were carried out using SEM in combination with EDX. The phases present in the samples after corrosion were studied using XRD.

In this investigation, galvanized steel sheets of types A, B, and C are referred to as Gal A, Gal B, and Gal C, respectively. Furthermore, in this study, the term steel substrate is referred to as uncoated steel.

3. Results and discussion

3.1 Characterization of the steel substrates and galvanized steels

SEM micrographs of the top surface of the steel substrates are shown in Fig. 1, microstructures of all the annealed steel substrates showed mainly ferrite grains. The steel substrate of Gal B had ~ 6.5 vol. % pearlite (Fig. 1 (b)) due to its slightly higher carbon content (Table 1).

Fig. 2 shows the SE-micrographs obtained from the coated top surfaces of all three GI sheets. The top surface of the Gal A and C coatings had surface defects such as attachment of dross particles and bare spots (Fig. 2 (a, c)), which could be due to process defects generated during the hot-dip galvanizing operation [1].

Compared to Gal A and Gal C (Fig. 2 (a, c)), the top coating surface morphology of Gal B was homogenous with negligible surface flaws except for scratches at a few places due to inappropriate handling in plant, as shown in Fig. 2 (b). To confirm the eta (η) phase in the GI coating, XRD analysis was performed. The XRD patterns clearly revealed the presence of a predominant η phase in the coating of all the GI sheets (Fig. 2 (d)). In addition, oxides and other minor phases are likely to exist on the surface of the coating, though, their presence is beyond the detection limit of XRD.

EDX elemental maps (Figs. 3 (a-o)) show the distribution of Fe, Zn, Al, and O across the cross-section of the three GI sheets. In all the coated

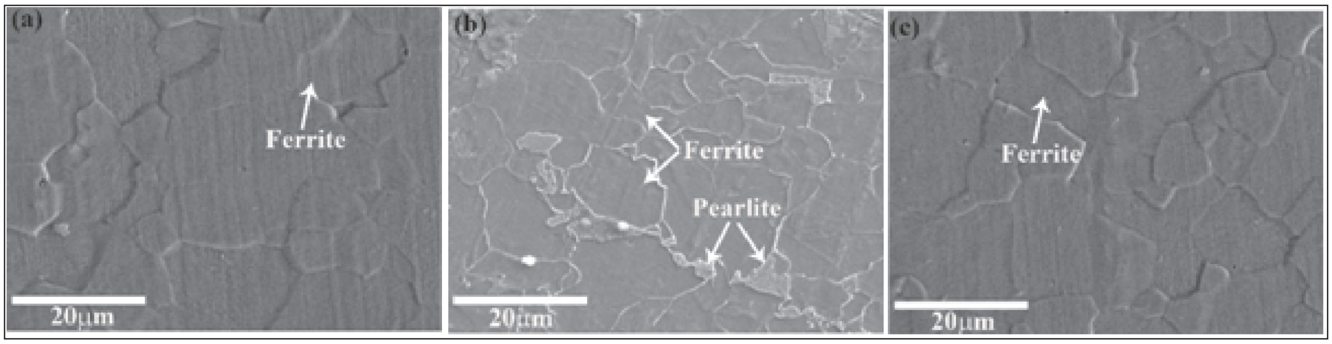

Fig. 1 : SE micrographs of steel substrate of (a) Gal A, (b) Gal B, and (c) Gal C.

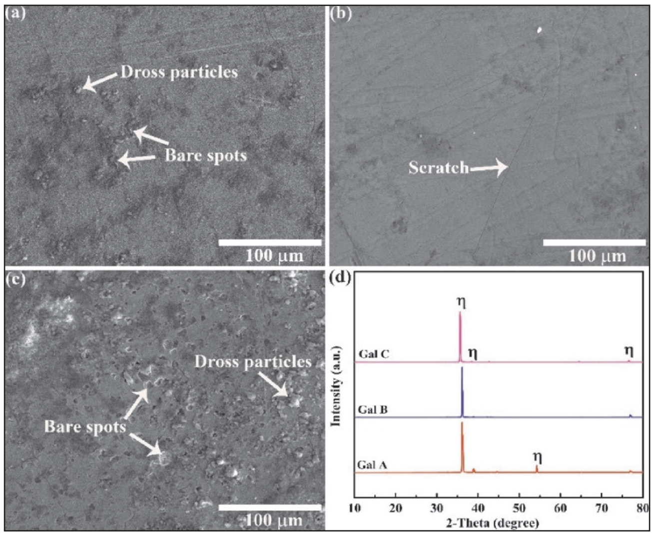

Fig. 2: SE micrographs of the top surface of coating specimens (a) Gal A, (b) Gal B, and (c) Gal C. (d) XRD patterns of all the GI sheets.

samples, EDX maps show a high concentration of Zn throughout the coating layer. For the coatings of Gal A and C, a very thin Al-rich layer was observed at the substrate-coating interface, indicating the layer to be continuous (Fig. 3 (d) and (n)), as also observed in previous studies [1, 4]. In contrast, the lack of Al at the substrate-coating interface in Gal B suggests the presence of diffused inhibition layer (incomplete formation of the inhibition layer) (Fig. 3 (i)), which could not stop the formation of Fe-Zn intermetallic phases at the substrate-coating interface. The presence of Fe-Zn intermetallic compound, in the form of zeta (ξ-$FeZn_{13}$) crystals, has been observed by many researchers for low carbon steels galvanized using a low Al-containing Zn-bath [1, 4, 10]. This could be due to formation of discontinuous Fe-AL inhibition layer at the substrate-coating interface.

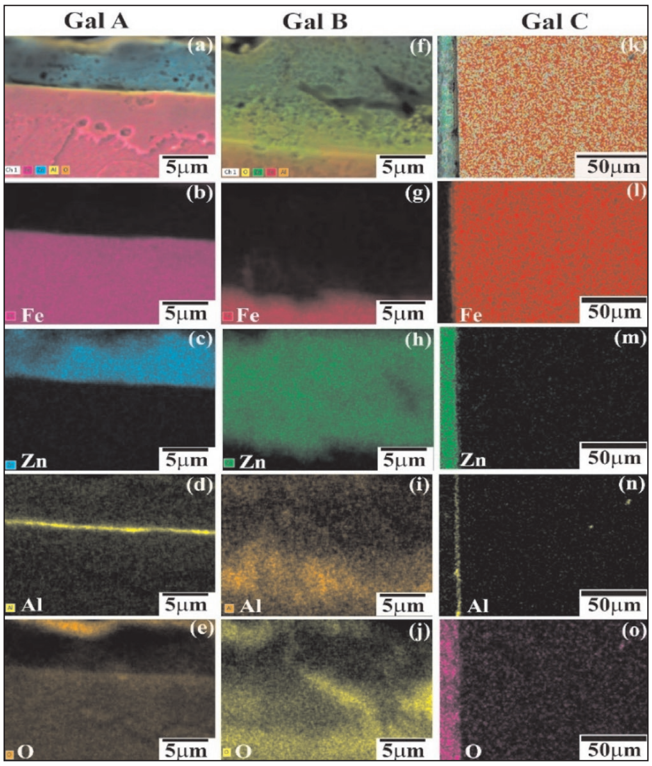

Fig.3 : EDX maps of the coating cross-sections of (a-e) Gal A, (f-j) Gal B, and (k-o) Gal C.

SE micrographs of cross-sections of all the coated specimens are shown in Fig. 4. The transverse sections of the coating morphologies of Gal A and C specimens showed only a single phase (eta (η) layer with an extremely thin continuous Fe-Al inhibition layer at the interface between substrate and coating (Fig. 4 (a, c)), as confirmed by EDX maps (Fig. 3 (a-e) and (k-o)). The coating of the specimen Gal B consisted of two distinct layers (Fig. 4 (b)) with the diffused Fe-Al inhibition layer at the interface, as confirmed by EDX maps (Fig. 3 (f-j)). The coating microstructure demonstrated the formation of familiar blocky morphology of zeta (ξ-$FeZn_{13}$) Fe-Zn crystals adjacent to the inhibition layer along with the overlay eta (η) phase [1, 10].

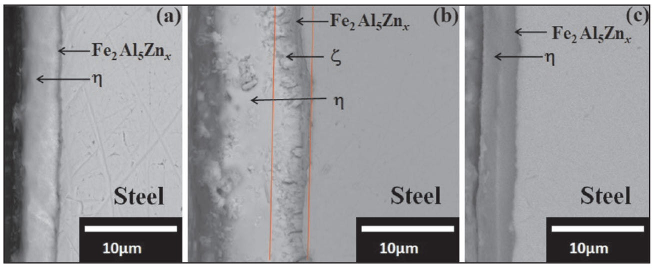

Fig. 4 : SE micrographs of the cross-sections of the coating specimens (a) Gal A, (b) Gal B, and (c) Gal C

For comparison, higher magnification SE micrographs of cross-sections of the coated specimens of Gal A and B are shown in Fig. 5. There were blocky crystals of zeta (ξ-$FeZn_{13}$) Fe-Zn intermetallic phase at the interface which grew into eta (η) only in the coating of Gal B (Fig. 5 (b)). In Gal A (Fig. 5 (a)), the formation of Fe-Zn intermetallic compounds in the coating was hindered by the formation of a very thin continuous interfacial layer of $Fe_2Al_5Zn_x$ between the substrate and coating. The reaction between liquid Zn and steel substrate was delayed due to the immediate formation of the iron-aluminide layer on the substrate surface as soon as the strip entered the liquid Zn-alloy bath. This is due to Fe having a stronger affinity for Al than Zn [1, 10]. Therefore, the final coating microstructure was composed of a very thin continuous layer of $Fe_2Al_5Zn_x$ covered with an overlay Zn layer without the formation of any Fe-Zn intermetallic phases.

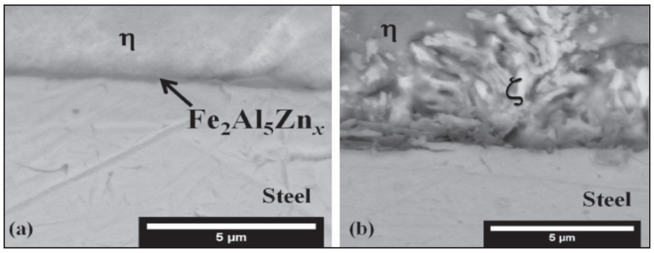

Fig. 5: SE micrographs of samples complete and incomplete Al-rich inhibition layer at substrate coating interface of steel of (a) Gal A and (b) Gal B.

In contrast, there was an incomplete barrier ($Fe_2Al_5Zn_x$ layer) at the substrate-coating interface in the coating of Gal B. This may have been due to insufficient availability of dissolved Al at the interface between the steel substrate and liquid Zn alloy leading to the formation of Fe-Zn intermetallic compounds in the coated structure. Based on the Fe-Zn equilibrium phase diagram [11], different Fe-Zn intermetallic compounds can form at the steel/coating interface when the steel substrate interacts with a molten Zn bath. The formation mechanism of Fe-Zn intermetallic compounds across the inhibition layer has been proposed by many investigators [1, 10]. In the Al depletion model [1, 10], Fe-Zn intermetallic compounds are expected to form between the molten Zn and the inhibition layer interface, while in the Zn diffusion model [1, 10], Fe-Zn intermetallic compounds are expected to form between the inhibition layer and substrate interface. In this study, the formation of Fe-Zn intermetallic compounds at the inhibition layer and substrate interface followed the Zn diffusion model. Due to the discontinuous inhibition layer at the interface from a lack of Al, molten Zn would directly react with the substrate, resulting in the formation of Fe-Zn intermetallic compounds, which would prevent further lateral growth of the inhibition layer [1, 10].

Furthermore, because carbon was present in the steel substrate of Gal B as lamellar pearlite (~ 6.5 vol. %), the rate of zeta (ξ-$FeZn_{13}$) Fe-Zn phase formation during galvanization was accelerated due to the increased surface area on which the reaction would take place (Fig. 1 (b)) [1, 3]. This is also thought to be the cause for the emergence of the zeta (ξ-$FeZn_{13}$) Fe-Zn phase at the interface, as well as the increased amount of Al diffused into the coating from the interface (Fig. 3 (i)) [1, 10]. Among the 3, the coating thickness of the steel of Gal B was the highest, which might be due to the variation in process parameters during hot-dip galvanizing, such as steel strip speed, knife gas pressure, dipping time, and Zn-bath temperature as well as the composition of the Zn-alloy bath [1, 12]. The presence of zeta (ξ-$FeZn_{13}$) phase in steel of Gal B also contributed towards an increase in the thickness of the coating due to its higher specific volume [1, 5]. Gal A and C steels had approximately the same Zn-coating thickness and structure.

3.2 Electrochemical experiments in a freely aerated 3.5 wt. % NaCl solution

3.2.1. Tafel polarization

Fig. 6 illustrates the comparative Tafel polarization plots of GI sheets (Gal A, B, and C) along with the steel substrates in freely aerated 3.5 wt. % NaCl solution. The electrochemical parameters, such as corrosion potential (E_{corr}, V_{SCE}), corrosion current density (i_{corr}, $\mu A/cm^2$), and corrosion rate (mm/year) values, are given in Table 2. The cathodic slope of the polarization plots indicates whether the reaction is controlled by diffusion or activation. In a freely aerated neutral 3.5 wt. % NaCl solution, hydrogen evolution is limited, and oxygen reduction is the primary cathodic process as revealed by the cathodic section of all the samples revealed diffusion-controlled behavior [13]. Therefore, the values of i_{corr} for all of the samples were taken as the limiting current densities of the oxygen reduction reaction, and the corrosion rates were calculated.

Fig. 6 (a-c) shows the Tafel polarization plots of coatings of Gal A, B, and C with the steel substrates. GI sheet curves were shifted slightly to the right compared to the steel substrate curves of each sample, suggesting that GI sheets had higher corrosion rates than steel substrates. Furthermore, the corrosion potential (E_{corr}) values of the GI sheets were always on the negative side compared to the steel substrate, which was attributed to the sacrificial nature of the

Zn coating. The same behavior of the coating and the steel substrate had been observed previously [14, 15]. The corrosion potential difference of ~ 0.31 V between the GI sheets and steel substrates was sufficient to form an effective galvanic coupling between them (Table 2) as the corrosion potential difference of ~ 0.1V has been found to be generally sufficient to form a galvanic couple [14, 15]. This also indicated that the Zn coating can prevent the underlying steel substrate from corrosion in a corrosive environment.

Table 2: Electrochemical parameters of GI sheets along with the steel substrates in a freely aerated 3.5 wt. % NaCl solution

Sample name	E_{corr} (V_{SCE})	i_{corr} (μA/ cm²)	Corrosion rate (mm/a)
Gal A	-1.044	19.85	0.297
Gal B	-1.044	13.52	0.202
Gal C	-1.045	18.98	0.285
Steel substrate of Gal A	-0.725	11.15	0.129
Steel substrate of Gal B	-0729	12.60	0.146
Steel substrate of Gal C	-0.722	11.30	0.131

The anodic polarization curves of all the GI sheets (Fig. 6 (d)) suggest the active dissolution of Zn coating over steel. The dissolution reaction of all the GI sheets proceeded rapidly as all anodic polarization curves are nearly horizontal to the current axis over a range of anodic current density [15]. The coatings of Gal A and C show approximately the same corrosion rate values (Table 2) due to their similar coating surface with noticeable defects. The coating of Gal B has a slightly lower corrosion rate than the coatings of Gal A and C (Table 2). The increase in corrosion resistance of coating of Gal B is due to a defect-free coating surface. Similar results have also been reported by Dong et al. [7] for galvanized low carbon steels in an aqueous environment. On the other hand, the corrosion rate of the steel substrate of Gal B was slightly higher than A and C (Table 2), owing to the existence of pearlitic colonies (~ 6.5 vol. %) in the ferrite matrix, which gave some sites for pearlite and ferrite to cause micro-galvanic corrosion. Prvan et al. [13] showed that pearlite acted as a cathodic part when it is connected with pro-eutectoid ferrite. Moreover, they also showed that within pearlite, cementite acted as cathodes, and ferrite lamellae were anodes. Furthermore, the anodic dissolution of the lamellar ferrite phase (anode) occurred in the pearlite colony, leaving behind a lamellar cementite phase (cathode). As a result, in the case of the steel substrate of Gal B, the overall dissolution of pearlite has also occurred.

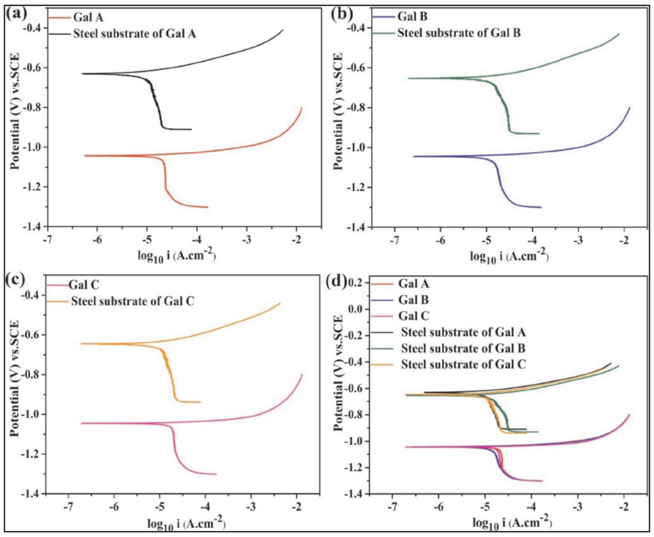

Fig. 6: Tafel polarization plots of coatings along with the steel substrate of (a) Gal A, (b) Gal B, and (c) Gal C. (d) Comparison of all the GI sheets and substrates of Gal A, B, and C

3.2.2 Characterization of corrosion surfaces after Tafel polarization

The surface morphologies of the coatings of Gal A, B, and C, after the Tafel polarization tests in a freely aerated 3.5 wt. % NaCl solution, are displayed in Fig. 7. The coatings of the samples Gal A and C suffered significant corrosion with visible cracks and damage in terms of pits (indicated by arrows) on the coating surface (Fig. 7 (a, e)). The EDX line scan of the corroded surfaces of Gal A and C (Fig. 7 (b, f)) shows Zn, Cl, and O indicating hexagonal crystal plates to be predominantly Zn corrosion product, possibly simonkolleite ($4Zn(OH)_2.ZnCl_2$) with zinc hydroxide (($Zn (OH)_2$) and zinc oxide (ZnO), which have also been observed in the earlier study during corrosion of Zn-coated steels [14, 15]. The coating of the specimen Gal B (Fig. 7 (c)) suffered significantly less coating damage compared to Gal A and Gal C. As expected, the corresponding line scan analysis of the corroded surface (Fig. 7 (d)) also shows the presence of Zn, Cl, and O. Furthermore, because of the Fe-Zn intermetallic zeta (ξ-$FeZn_{13}$)

phase and distributed Al in the coating, EDX line scan revealed that the Fe and Al signals in Gal B were stronger than those in Gal A and Gal C. Also, it is crucial to understand that the Fe present on the Gal B coating surface following corrosion is a result of the Fe-Zn intermetallic zeta (ξ-$FeZn_{13}$) phase, not the steel substrate.

After Tafel polarization tests, XRD was performed on the GI sheets to confirm the corrosion products on the coated surface. Fig. 8 shows the peaks corresponding to $4Zn(OH)_2.ZnCl_2$ (simonkolleite) (JCPDS card No. 1713500), $Zn(OH)_2$ (JCPDS card No. 1625667), and ZnO (JCPDS card No. 529027) on all the GI sheets corroborating with the EDX line scan analysis (Fig. 7). Furthermore, due to the presence of the Fe-Zn intermetallic zeta (ξ-$FeZn_{13}$) phase and dispersed Al in the coating, the EDX line scan of the Gal B showed associated Fe and Al signals (Fig. 7 (d)), which were not detectable by XRD due to their low volume fraction compared to the Zn-based corrosion products.

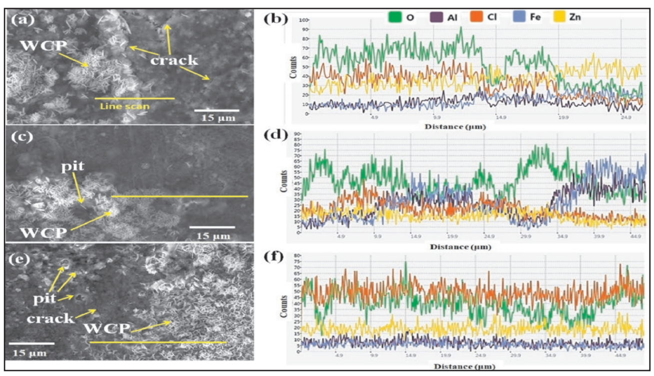

Fig. 7 : SE micrographs of the corroded coating surface of (a, b) Gal A with corresponding line scan, (c, d) Gal B with corresponding line scan, and (e, f) Gal C with corresponding line scan. [WCP = White Corrosion Products].

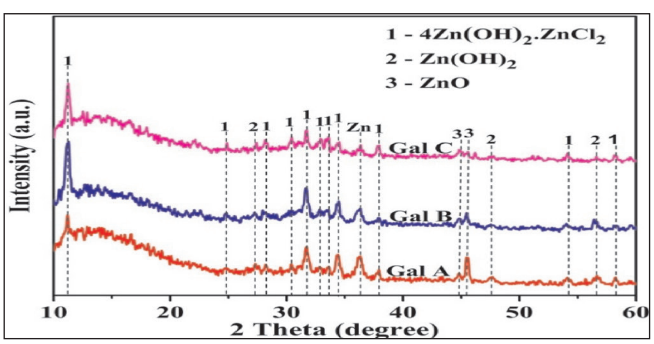

Fig. 8 : XRD patterns of all the GI sheets after Tafel polarization.

Some studies have shown that increasing the proportion of the simonkolleite phase in corrosion products improved corrosion resistance [14, 15]. In the current investigation, the phase fraction of simonkolleite was determined from the XRD patterns of all the GI sheets to understand the role of this phase in the corrosion products. All the XRD peaks' relative intensities were normalized, and baseline correction was done using OriginPro software before estimating the phase fraction of simonkolleite. The simonkolleite phase fraction was estimated by dividing the sum of the area of the XRD peaks corresponding to the simonkolleite phase by the entire sum of the area of all the peaks in the XRD pattern. Gal B had a slightly higher simonkolleite phase fraction (86 %) than Gal A (80 %) and Gal C (82 %), implying that Gal B should have better corrosion resistance than Gal A and Gal C. The corrosion rate data obtained after Tafel polarization tests for all GI sheets (Fig. 6 and Table 2) showed a good correlation with the variation of simonkolleite phase fraction.

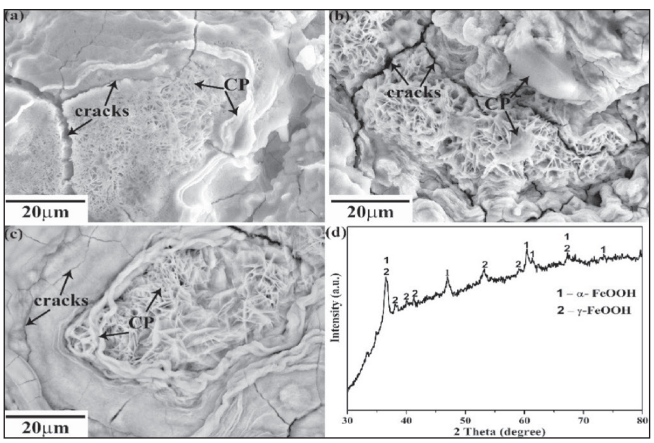

Fig. 9: SE micrographs of the surface of steel substrate after corrosion for (a) Gal A, (b) Gal B, and (c) Gal C. (d) Representative XRD pattern of steel substrates after corrosion. [CP = corrosion product].

Fig. 9 (a-c) shows the surface morphologies of steel substrates of Gal A, B, and C after the Tafel polarization test in a freely aerated 3.5 wt. % NaCl solution. It is clear that all the steel substrates suffered general corrosion with visible cracks on the surfaces. The corroded surfaces of all the steel substrates were covered with corrosion products (CP). Figure 9 (d) shows a representative X RD pattern of the corroded surface of the steel substrates following the Tafel polarization test, demonstrating that the corrosion products on all steels were α-FeOOH (JCPDS card No. 1819113) and γ-FeOOH (JCPDS card No. 1122427).

4. Conclusions

- A very thin inhibition layer ($Fe_2Al_5Zn_x$) was observed at the substrate-coating interface of Gal A and C steels, which prevented iron diffusion from steel to the zinc coating during galvanization.
- Fe-Zn intermetallic zeta (ξ-$FeZn_{13}$) phase formation at the substrate-coating interface of Gal B steel was due to insufficient Al at the interface. The presence of the zeta (ξ-$FeZn_{13}$) phase in the coating structure led to an increase in the thickness of the Gal B steel, as shown by its higher specific volume.
- The corrosion rate of the steel substrate increased noticeably with C content from 0.045 (Gal A and C) to 0.07 wt. % (Gal B) because of the existence of pearlite colonies.
- The corrosion potential difference of ~ 0.31 V between the GI sheets and steel substrates is expected to be sufficient to form an effective galvanic coupling between them to suppress corrosion of steel substrates.
- The coating of Gal B had a higher corrosion resistance than Gal A and C because of its defect-free coating surface.
- After polarization in a freely aerated 3.5 wt. % NaCl solution, the corrosion products simonkolleite, zinc hydroxide, and zinc oxide were typically seen over the entire GI sheet surface, and the corrosion products α-FeOOH and γ-FeOOH on the steel surface.

References

1. A.R. Marder, The metallurgy of zinc-coated steel, Prog. Mater Sci., 2000, 45, p 191-271.
2. M.S. Noor Idora, M.M. Rahman, M. Ismail, W.B. Wan Nik, Effect of Zn coating thickness on corrosion performance of mild steel in atmospheric and seawater environment, Appl. Mech. Mater., 2014, 554, p 213-217.
3. P. Pokorny, J. Kolisko, L. Balik, P. Novak, Effect of chemical composition of steel on the structure of hot-dip galvanized coating, Metalurgija, 2016, 55, p 115-118.
4. G.K. Mandal, S.K. Das, R. Balasubramaniam, S.P. Mehrotra, Evolution of microstructures of galvanized and galvannealed coatings formed in 0.2 wt. % aluminum-zinc bath, Mater. Sci. Technol., 2011, 27, p 1265-1270.
5. H.E. Townsend, Continuous hot-dip coating in surface engineering, ASM handbook, Tenth edition, 1994, 5, p 339.
6. A.P. Yadav, H. Katayama, K. Noda, H. Masuda, A. Nishikata, T. Tsuru, Effect of Fe–Zn alloy layer on the corrosion resistance of galvanized steel in chloride containing environments, Corros. Sci., 2007, 49, p 3716–3731.
7. C.F. Dong, A.Q. Fu, X.G. Li, Y.F. Cheng, Localized EIS characterization of corrosion of steel at coating defect under cathodic protection, Electrochim. Acta, 2008, 54 (2), p 628–633.
8. R. Vera, F. Guerrero, D. Delgado, R. Araya, Atmospheric corrosion of galvanized steel and precipitation runoff from zinc in a marine environment, J. Braz. Chem. Soc., 2013, 24, p 449-458.
9. ASTM G102-89, Standard practice for calculation of corrosion rates and related information from electrochemical measurements, ASTM International, West Conshohocken (1999).
10. G.K. Mandal, D. Mandal, S.K. Das, R. Balasubramaniam, S.P. Mehrotra, Microstructural study of galvanized coatings formed in pure as well as commercial grade zinc baths, Trans. Indian Inst. Met., 2009, 62, p 35-40.
11. N.Y. Tang, Characteristics of continuous-galvanizing baths, Metall. Mater. Trans. B, 1999, 30B, p 144-147.
12. A.P. Deote, M.M. Gupta, D.R. Zanwar, Process parameter optimization for zinc coating weight control in continuous galvanizing line, Int. J. Sci. Eng. Res., 2012, 3.
13. P.K. Katiyar, S. Misra, K. Mondal, Corrosion behavior of annealed steels with different carbon contents (0.002, 0.17, 0.43 and 0.7% C) in freely aerated 3.5% NaCl solution, J. Mater. Eng. Perform., 2019, 28, p 4041–4052.
14. H. Kancharla, G.K. Mandal, S.S. Singh, K. Mondal, Effect of strip entry temperature on the interfacial layer and corrosion behavior of galvanized steel, Surf. Coat. Technol., 2022, 433, p 128071-128085.
15. H. Kancharla, G.K. Mandal, S.S. Singh, K. Mondal, Effect of prior copper-coating on the microstructural development and corrosion behavior of hot-dip galvanized Mn containing high strength steel sheet, Surf. Coat. Technol., 2022, 437, p 128347.

****

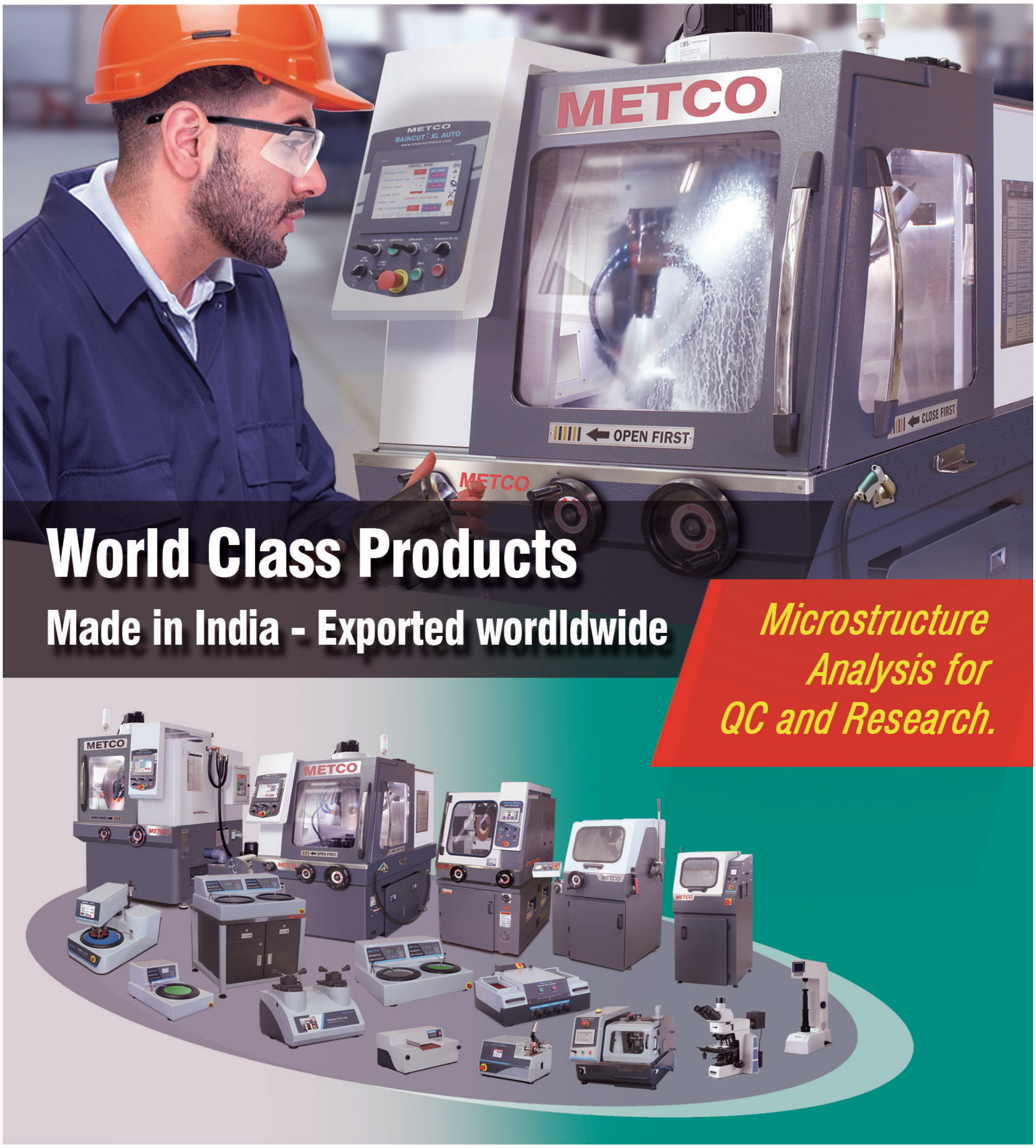
METCO
OPEN FIRST
CLOSE FIRST
World Class Products
Made in India - Exported wordldwide
Microstructure Analysis for QC and Research.
METCO

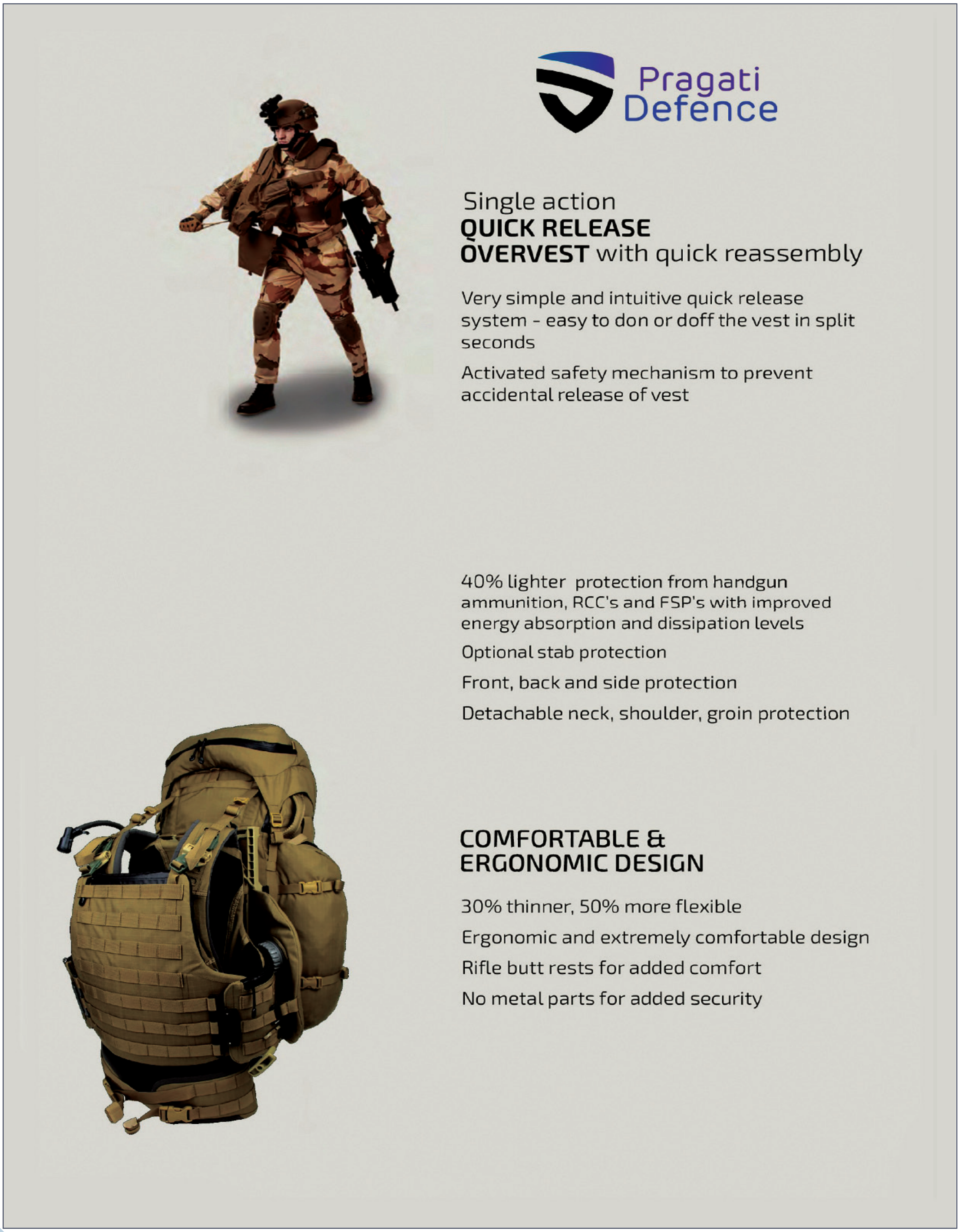
Pragati Defence
Single action
QUICK RELEASE
OVERVEST with quick reassembly
Very simple and intuitive quick release system - easy to don or doff the vest in split seconds
Activated safety mechanism to prevent accidental release of vest
40% lighter protection from handgun ammunition, RCC's and FSP's with improved energy absorption and dissipation levels
Optional stab protection
Front, back and side protection
Detachable neck, shoulder, groin protection
COMFORTABLE &
ERGONOMIC DESIGN
30% thinner, 50% more flexible
Ergonomic and extremely comfortable design
Rifle butt rests for added comfort
No metal parts for added security

रक्षा अनुसंधान एवं विकास संगठन
रक्षा मंत्रालय, भारत सरकार
DEFENCE RESEARCH & DEVELOPMENT ORGANISATION
Ministry of Defence, Government of India

Aeronautics Research & Development Board

Vision

Make India technologically strong by establishing world class cutting edge aeronautical science and technology base to provide our Defence, Space and Civil Aviation sectors a decisive edge by equipping them with internationally competitive systems and solutions.

Mission

To encourage and fund basic and applied research in pertinent scientific disciplines directly relevant to our aeronautical systems needed for future by enabling and supporting emerging talents, particularly in academic and research institutions to create and evolve a potential knowledge-base system applicable to future aeronautics needs of the country.

Charter

- To formulate research, design and development programmes in aeronautics and allied sciences, keeping in view future needs of the country specifically with respect to aircraft, helicopter, missiles and all other airborne vehicles.
- To implement such programmes through appropriate institutions and individuals by sponsoring research, design and development projects, creating/ improving infrastructure facilities deemed necessary, while ensuring that they are suitably monitored.
- To promote in all possible ways such educational and training programmes as may be considered necessary for ensuring that adequate manpower of requisite quality becomes available to various aeronautical organizations in the country.
- To promote all relevant R&D activities in the country through appropriate scientific meetings, provisions of support for participation of Indian and foreign scientists in such meetings, conduct of relevant competitions as well as other training and visiting programmes within India and abroad as may fall within the scope of the programmes mentioned at sub para (a) above.
- Dissemination of appropriate technical information through journals and documents, encouragement of individual and collective efforts and nurturing of young talent by institutions with suitable awards, scholarships etc. Organization of necessary centralized services related documentation, software, data-link etc. and in all such other ways that the Board may determine from time to time.

Panels & Chairman	
Aerodynamics Panel **Dr S Pandian** Prof. Vikram Sarabhai Distinguished Professor & Ex- Director & DS, SHAR	**Propulsion Panel** **Dr V Ramanujachari** National Centre for Combustion Research & Development (NCCRD), IIT Madras, Chennai
Aerospace Resources Panel **Dr N Eswara Prasad** OS & Director, DMSRDE (DRDO), Kanpur-13	**UNMANNED AERO SYSTEMS PANEL** **Shri PS Krishnan** DS & Ex-Director, ADE, Bangalore-560075
Materials & Manufacturing Panel **Dr DK Das, Scientist H** Group Head (DSG), DMRL (DRDO) Hyd. - 58	**Structures Panel** **Dr Makarand Joshi** Scientist G, R&DE (E), DRDO, Pune-411015
GTMAP **Prof. Amol A Gokhale, IITB, Chairman**	**Systems / Systems Engineering Panel** **Shri APVS Prasad** Scientist H, CE, CEMILAC, DRDO, Bangalore

News Updates National

Vedanta to move towards green steel; working on solution for hydrogen use

As part of its plan to shift towards "green steel", a Vedanta group firm has said it is working on a solution to use hydrogen instead of coke in its manufacturing process so as to reduce carbon emissions.

Vedanta's Sesa Goa Iron Ore Business said it is looking for a tie-up with IIT-Bombay to carry out a research for manufacturing pig iron ore using hydrogen in place of coke. The solution is aimed at reducing carbon emission in the production process and will help manufacture green steel (an outcome of a climate-friendly process).

"We have our own vision of going towards the green steel. So my coke ovens will become green coke very soon, where I will be having all the coke-making through a green process, extracting, harnessing... and it will simply float over the grid. I would not require power from the grid, rather I would give power to the grid," Sujal Shah, Deputy CEO, Vedanta's Sesa Goa Iron Ore Business, told PTI in an interview.

Business Standard

'Boron' involves rescue of metal corporations hit by export levy

At a time when a brand new 15% export obligation on metal has introduced sale of the alloy abroad underneath strain, one exception has come to the rescue of Indian metal mills within the type of boron, a brownish darkish powder that makes metal more durable and, extra importantly, brings it out of the purview of the brand new levy.

The exports {of electrical} metal, which incorporates boron-added alloy metal, grew eightfold yr on yr to about 1,40,000 tonnes through the fiscal first quarter ended June, as per knowledge from SteelMint.

By one estimate, about 1,30,000 tonnes of those exports occurred in June, following the levy of the brand new export obligation from May 22. This compares to the general metal exports of 6,40,000 tonnes in June.

"If there are customers who are willing to accept some amount of boron in the steel, then for such customers prices remain competitive and not have this extra levy of 15%," mentioned TV Narendran, CEO and Managing Director of Tata Steel. "So that's how some of the exports have happened."

To make sure, some exports of metal additionally occurred after paying the 15% obligation as not all clients had been keen to just accept boron-added metal – particularly for vital long-standing clients that steelmakers would not wish to lose, for the reason that export obligation is anticipated to be a brief measure.

The Indian authorities introduced speedy imposition of the export obligation in May to rein in home metal costs in its effort to comprise inflation. Following the levy, exports of metal in June declined to a half in comparison with the previous year.

The Economic Times

India's steel output grows 6% to 10 Mt in June, shows worldsteel data

India's crude steel production rose over 6% year-on-year to 10 million tonnes in June 2022, according World Steel Association. As per the WSA (worldsteel) data, India is the only country which has registered a positive growth in its steel output during June. The country had produced 9.4 million tonnes (Mt) crude steel during the same month last year, the global industry body said in its latest report.

India is world's second largest producer of crude steel after China which produced 90.7 Mt in June 2022, down 3.3 per cent over its 93.9 Mt production in June 2021.

Business Standard

India's exports grow 25 per cent to 13.49 Mt in FY22; imports fall 1.68 per cent to 4.67 Mt: Minister Kulaste

The exports of finished steel from India jumped over 25 per cent to 13.49 million tonne (Mt) in 2021-22, Union Minister Faggan Singh Kulaste said.

During the preceding 2020-21 fiscal, the exports stood at 10.78 Mt, the Minister of State for Steel said to the Lok Sabha. The imports fell to 4.67 Mt in 2021-22 from 4.75 Mt a year ago, a fall of 1.68 per cent, according to Kulaste.

"Government has taken various steps to increase the availability of iron ore and make them available at reasonable prices, which, inter-alia, including Mining and Mineral Policy reforms to enhance production/availability of iron ore," he said.

Financial Express

Jindal Stainless to supply 3,500 tonnes steel for USBRL tunnel project

Jindal Stainless will supply 3,500 tonnes stainless steel for the Indian Railway's Udhampur-Srinagar-Baramulla Railway Link (USBRL) tunnel project coming up in Jammu and Kashmir.

In a statement, the company said the project is a 272 km-long railway link between Jammu and Kashmir. This will be the first-ever application of stainless steel cable trays in an Indian railway project, the company said.

"USBRL will be a milestone in improving the economic landscape of J&K. We congratulate Railways on executing the engineering marvel by overcoming various topographical challenges, and appreciate its decision to choose stainless steel for developing a sustainable railway infrastructure," JSL Managing Director, Jindal Stainless, Abhyuday Jindal said.

According to the statement, company's arm Jindal Stainless Steelway Ltd will supply "EN 1.4404/316L (dual certification) stainless steel grade in 2B finish" for the project owing to its high corrosion resistance, high strength-to-weight ratio, and a lower life cycle cost.

USBRL is the highest altitude railway network and the most challenging railway project undertaken by the Indian Railways. The newly constructed railway line will provide an all-weather and reliable connectivity to Jammu and Kashmir.

Business Standard

JSW Steel ropes in BCG to work on decarbonization goals

JSW Steel said it has partnered with US-based Boston Consulting Group (BCG) to meet its decarbonization goals. JSW Steel has an ambitious target of reducing its carbon emission by 42 per cent by 2029-30 versus base year 2005.

According to a ministry document, the iron and steel industry globally accounts for around 8 per cent of total carbon dioxide (CO_2) emissions on an annual basis, whereas in India, it contributes 12 per cent to the total CO_2 emissions. Thus, the Indian steel industry needs to reduce its emissions substantially in view of the commitments made at the COP26 climate change conference.

The Economic Times

Tata Steel aims to restart NINL steel mill in next 3 months: Narendran

Tata Steel is aiming to restart the 1-million tonne (Mt) NINL steel mill in the next three months, CEO and MD Mr. T.V. Narendran said. Tata Steel completed the acquisition of NINL through its subsidiary Tata Steel Long Products (TSLP) for a consideration of ₹12,000 crore. The Odisha-based plant has been closed for almost two years.

"We are ready to work with existing employees and restart the plant which has been closed for almost 2 years. We hope to get the production started in the next 3 months and ramp up to the rated capacity over the next 12 months," the top official said.

The Hindu

Tata Steel reports decent Q1 production nos

Tata Steel India business reported 6% rise in crude steel production to 4.92 million tons in Q1 FY23 from 4.63 million tons posted in Q1 FY22. Sequentially, crude steel production rose marginally from 4.90 million tons in Q4 FY22.

Deliveries stood at 4.06 million tons in Q4 FY23, lower by 2% year on year (YoY) and a fall of 20.7% quarter on quarter (QoQ), due to moderation in exports following the imposition of 15% export duty. However, Domestic deliveries were ramped up leveraging our strong marketing network & agile business model and increased by 5% YoY.

Business Standard

Chapter Activities: Kanpur, Kalpakkam, Mumbai, Raigarh, Trivandrum, Vijaynagar, Bokaro, Keonjhar

Kanpur Chapter

IIM Kanpur chapter organised two technical talks which are as follows :

1. On June 30, 2022 Dr. Anirban Patra, Department of Metallurgical Engineering and Materials Science, IIT Bombay presented the talk on “Strain Gradient Plasticity Modeling of Grain-Scale Deformation Phenomena”.

2. On July 8, 2022 Dr. Ilaksh Adlakha, Department of Applied Mechanics, IIT Madras delivered the talk on “First-principles investigations into the electrochemical behavior of Mg based intermetallics”.

Kalpakkam Chapter

IIM Kalpakkam chapter organised three technical lectures in the month of July at IGCAR Kalpakkam.

1. On 6th July, 2022 Dr. R. N. Singh, BARC, Mumbai delivered the lecture on ‘Manufacture of Zr-2.5Nb alloy pressure tubes’.

2. Dr. Aniruddha Biswas, BARC, Mumbai delivered the lecture on July 18, 2022 on the topic ‘Case studies of quantitative evaluation of nanoscale phase separation in Fe-Cr system using combinatorial APT & SANS analyses’.

3. And on 21st July, 2022 Dr. Sairam K Malladi, IIT Hyderabad delivered the lecture on ‘Challenges and opportunities with in-situ electron microscopy: Heating, Environmental and Liquid Cells’.

Mumbai Chapter

On 4th July, 2022 the Mumbai Chapter organised the evening lecture on “Wear Resistance and Corrosion Protection”. The Speaker of the lecture was Dr. Mohammad Umar Farooq Khan, Post-Doctoral Researcher, Texas A&M University.

Raigarh Chapter

IIM Raigarh Chapter organised two events in the month of July.

1. On 22nd July, 2022 the chapter conducted the Executive committee Meeting in virtual mode,

2. On July 26, 2022 a technical talk on "Decarbonisation and Use of Hydrogen in Iron & Steel Making" was conducted. The Speaker of this web lecture was Mr. Praveen Chaturvedi, VP & Head – Sales Upstream India, Tenova Technologies Pvt. Ltd., India. Over 235 nos. of professionals attended this session from different IIM chapters virtually.

Trivandrum Chapter

IIM Trivandrum Chapter organised the lecture on “Role of Metallurgists in Indian Space Programme” on 11th March, 2022 to celebrate the foundation day of IIM (24th February). The lecture was delivered by Shri M Mohan, Deputy Director, Vikram Sarabhai Space Centre. More than 70 members attended the event which was conducted in Hybrid Mode.

Vijaynagar Chapter

IIM Vijaynagar Chapter organised the following lectures recently :

1. Dr. Matej Drobne, Research and Development, Vajli, Slovenia presented the lecture on 5th Apr, 2022. The topic of the lecture was “New Developments in Hot Strip Mill Rolls”.

2. On 24th May, 2022, Prof. Somnath Basu, Metallurgical Engineering and Material Science Dept, IIT Bombay delivered a talk on “BOF slag: From a solid waste to a medium for water purification”.

3. On 6th July, 2022, Mr. L R Singh, COO & Dr. Dhiren Panda, Head (EVP) R&D, JSW Steel Vijayanagar

Works delivered the lectures on the topic "Raising Steel Consumption: Ways to increase rural steel usage & way forward".

Bokaro Chapter

IIM Bokaro Chapter organised their Annual General Meeting on 1st June, 2022 at the Bokaro Club Limited, Bokaro Steel City. The meeting was convened to apprise the members of the chapter activities after a span of two years and to plan for the year ahead along with the election of the new executive committee members. The chapter website was also launched in that occasion. The executive committee for FY 2022-23 :

- Chairman : Shri Sanjay Kumar, ED(W), BSL
- Secretary : Shri Nityananda Mondal, CGM, RDCIS, Bokaro
- Treasurer : Smt. Biswasi Sunita, DGM (RCL), BSL

Keonjhar Chapter

The IIM Keonjhar Chapter conducted the AGM cum Technical session on 10th June, 2022 at Barbil. Three Technical sessions were organised with a participation of about 120 people from the Industries around the district of Keonjhar, Odisha.

Shri Shailendra Voleti delivering the lecture

- Dr. Ashok Kumar Sahu, Chief Scientist & Head, Mineral Processing Department Head, Strategic Planning & Business Development CEO, InTEC (Innovative & Technology Enabling Centre, a CSIR-IMMT Incubation Centre) delivered the lecture on "Recovery of Iron Values from lean & low grade resources".
- Shri Shailendra Voleti, Zonal General Manager Bhubaneshwar Zonal Office, Gas Authority of India Limited presented the lecture on "Thinking Beyond Conventional Fuels : Natural Gas Utilisation".
- Dr. Arup Kumar Samanta, AVP (Technology - Monolithics & RH Snorkel) TRL-KROSAKI Refractories Limited presented the lecture on "DRI & Pellet Plant - A holistic approach towards complete solution".

Dr. Ashok Kumar Sahu delivering the lecture

Dr. Arup Kumar Samanta delivering the lecture

****

Steel Statistics June 2022

Crude Steel production by region (June)

	Jun 2022 (Mt)	% change Jun 22/21	Jan-Jun 2022 (Mt)	% change Jan-Jun 22/21
Africa	1.2	-18.7	7.3	-9.1
Asia and Oceania	118.8	-3.1	701.4	-4.8
EU (27)	11.8	-12.2	73.8	-6.2
Europe, Other	3.8	-10.9	24.0	-5.0
Middle East	3.4	-5.0	20.4	-5.9
North America	9.6	-2.4	57.2	-2.3
Russia & other CIS + Ukraine	5.9	-34.3	43.6	-18.0
South America	3.7	-4.9	21.8	-2.8
Total 64 countries	**158.1**	**-5.9**	**949.4**	**-5.5**

The 64 countries included in this table accounted for approximately 98% of total world crude steel production in 2021.

Top 10 steel-producing countries

	Jun 2022 (Mt)	% change Jun 22/21	Jan-Jun 2022 (Mt)	% change Jan-Jun 22/21
China	90.7	-3.3	526.9	-6.5
India	10.0	6.3	63.2	8.8
Japan	7.4	-8.1	46.0	-4.3
United States	6.9	-4.2	41.1	-2.2
Russia	5.0 e	-22.2	35.4	-7.2
South Korea	5.6 e	-6.0	33.8	-3.9
Germany	3.2	-7.0	19.6	-5.5
Turkey	2.9	-13.1	19.0	-4.6
Brazil	2.9 e	-6.1	17.4	-2.9
Iran	2.2 e	-10.8	13.6	-10.8

e - estimated. Ranking of top 10 producing countries is based on year-to-date aggregate

Source : worldsteel.org

****

Advertisers' Index


STEEL FACTS
When taking a life cycle approach to compare
functionally equivalent automotive components,
Advanced High-Strength Steels consistently outperform lower density competing materials, emitting in the production phase
5 times less CO_2
than aluminium or carbon fibre, and
7 times less CO_2
than magnesium.
worldsteel.org


*Dow Jones Sustainable Indices 2020 & 2021